The Company of **Biologists**

Biology Open

RESEARCH ARTICLE

Development and validation of RdRp Screen, a crystallization screen for viral RNA-dependent RNA polymerases

Federica Riccio[1,‡], Sandeep K. Talapatra[1,*,‡,§], Sally Oxenford[2], Richard Angell[2], Michela Mazzon[3] and Frank Kozielski[1,§]

ABSTRACT

Members of the *Flaviviridae* family constitute a severe risk to human health. Whilst effective drugs have been developed against the *hepacivirus* HCV, no antiviral therapy is currently available for any other viruses, including the *flaviviruses* dengue (DENV), West Nile and Zika viruses. The RNA-dependent RNA polymerase (RdRp) is responsible for viral replication and represents an excellent therapeutic target with no homologue found in mammals. The identification of compounds targeting the RdRp of other flaviviruses is an active area of research. One of the main factors hampering further developments in the field is the difficulty in obtaining high-quality crystal information that could aid a structure-based drug discovery approach. To address this, we have developed a convenient and economical 96-well screening platform. We validated the screen by successfully obtaining crystals of both native DENV serotype 2 and 3 RdRps under several conditions included in the screen. In addition, we have obtained crystal structures of RdRp3 in complex with a previously identified fragment using both soaking and co-crystallization techniques. This work will streamline and accelerate the generation of crystal structures of viral RdRps and provide the community with a valuable tool to aid the development of structure-based antiviral design.

KEY WORDS: Dengue virus, Crystallization screen, RNA-dependent RNA polymerase, Flavivirus, Antiviral drug discovery

INTRODUCTION

Flaviviridae are a family of enveloped, positive single stranded RNA viruses. The genus *Flavivirus*, of the *Flaviviridae* family, counts over 70 different viruses (Fields et al., 2007; Kuno et al., 1998), including Dengue virus (DENV), Japanese encephalitis virus (JEV), tick-borne encephalitis virus (TBEV), West Nile virus (WNV), yellow fever virus (YFV) and Zika virus (ZIKV). Most of these viruses are arthropod-borne and can cause widespread morbidity and mortality. For instance, infection with DENV, which is estimated to affect 390 million people annually (Bhatt et al., 2013), can lead to an ample range of clinical manifestations, from mild fever to fatal dengue shock syndrome (Rajapakse, 2011), while infection with ZIKV has recently been shown to be responsible for the sudden surge in the number of cases of microcephaly and neurological abnormalities in new-borns, and for several cases of Guillain-Barré syndrome (Dyer, 2015; Oliveira Melo et al., 2016). No antivirals are currently available and vaccines are limited to YFV, JEV and TBEV. The vaccine currently licensed for DENV (Dengvaxia, Senofi-Pasteur) only has limited efficacy against some DENV serotypes, and concerns have been raised over its administration to children and seronegative individuals (Aguiar et al., 2016). In the absence of safe and effective vaccines, and given the risk of emergence of new flaviviruses, as demonstrated by the recent re-emergence of ZIKV, the development of antivirals against this group of viruses becomes ever more important.

The flavivirus genome of ∼11 kb is translated into a single polyprotein which is processed into three structural (envelope, membrane and capsid) and seven non-structural proteins (NS1, NS2A, NS2B, NS3, NS4A, NS4B, NS5). NS5 is the largest and most conserved protein, with members of the flavivirus genus sharing approximately 60–65% sequence similarity (Lim et al., 2015).

DENV NS5 (∼900 aa) is comprised of a methyltransferase (MTase) domain (∼250 aa) at the N-terminus, mainly responsible for RNA cap formation during viral replication (Egloff et al., 2002; Ray et al., 2006), and an RNA-dependent RNA polymerase (RdRp) domain at the C-terminus (∼600 aa). The RdRp is mostly known for its role in virus replication (Selisko et al., 2014). It functions by replicating the viral genomic +RNA into uncapped −RNA, leading to the formation of a double-stranded RNA intermediate, and then using the −RNA template to synthesize new +RNA copies of the viral genome (Malet et al., 2008). In addition, the RdRp plays an important role in escaping the host immune response by blocking IFN type I signalling through binding the transcription factor STAT2 and promoting its degradation (Ashour et al., 2009; Mazzon et al., 2009).

The overall structure of the RdRp domain consists of three main subdomains known as the 'fingers', 'palm' and 'thumb' (Fig. 1A). These subdomains are made up of seven conserved motifs (A to G) important for RNA binding and replication (Sousa, 1996; Malet et al., 2007; Yap et al., 2007). Motifs F and G are believed to interact with the RNA template (Iglesias et al., 2011) and with nucleoside triphosphates (NTP) (Sousa, 1996) for RNA elongation. It has been proposed that DENV RdRp undergoes a conformational change from a 'closed' initiation complex, bound to single-stranded RNA, to an 'open' elongation complex, bound to double-stranded RNA. Not surprisingly, sections of the flexible loops from motifs F (residues 455–468) and G (residues 406–417) are disordered and not observed in the apo-structures (Yap et al., 2007). Structures of
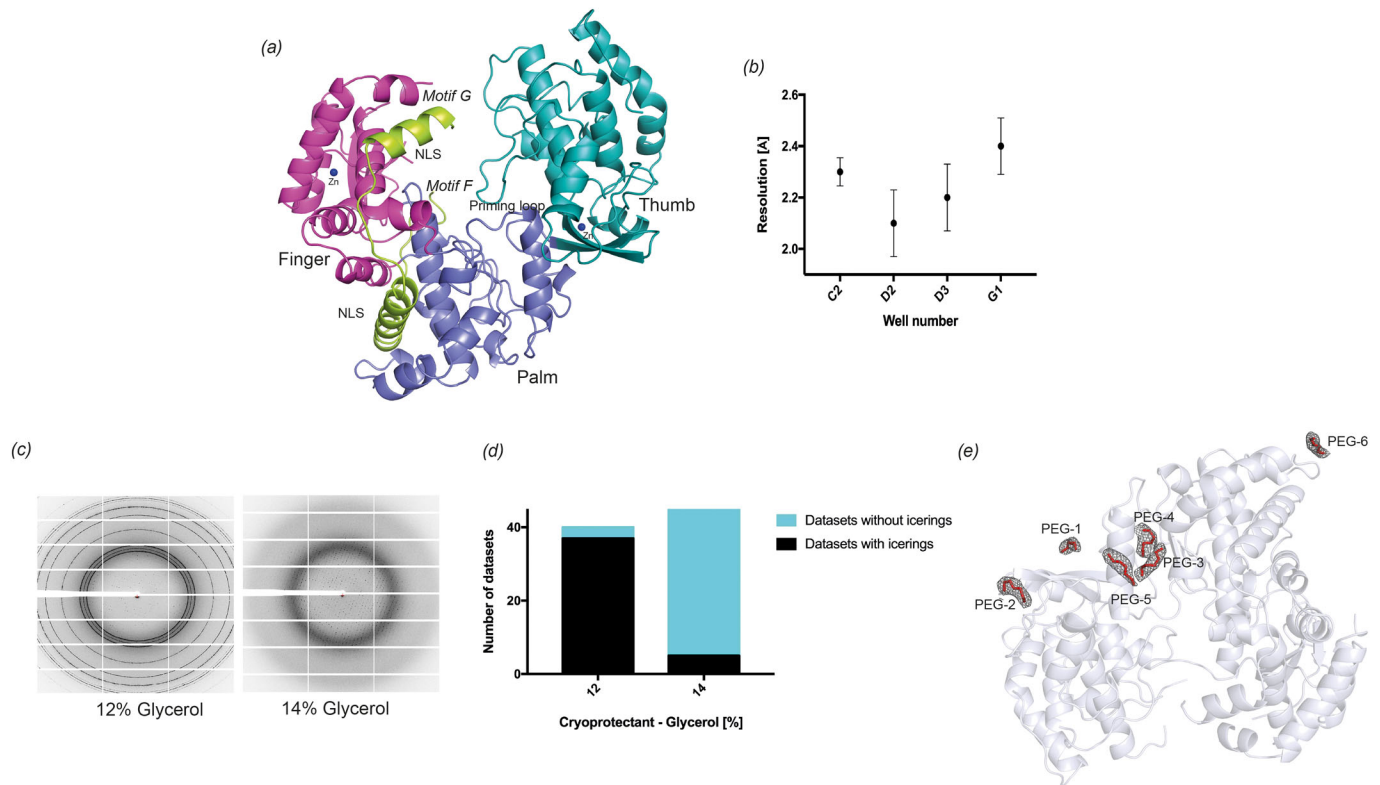
Fig. 1. Representative details of optimized cryo-conditions. The structure of dengue RdRp and the location of PEG-ions in the structure. (A) The overall structure of the RdRp domain of dengue virus serotype 3. The different secondary elements represent the thumb (turquoise), finger (magenta), palm (purple) and NLS regions (green). The two Zinc atoms are represented as blue spheres. (B) Representative diffraction pattern of RdRp crystals in the presence of either 12% glycerol or 14% glycerol as a cryoprotectant are shown. 12% glycerol shows ice rings correlated with a decrease in resolution, which prompted us to investigate 14% glycerol as a cryoprotectant (*n*=10, mean±s.d.). (C) Bar diagram of quantitative representation of number of datasets obtained with 12 (*n*=39) and 14% (*n*=41) glycerol as cryoprotectant that either had ice rings (black) or no ice rings (blue). (D) The PEG ions coordination and their electron density omit map (coloured in grey) contoured at 1 σ. The numbering of PEG is based on the number of PEG molecules present in different structures. For example, a structure with four PEG ions will contain PEG-1 to PEG-4. Figures B and C were prepared using PyMOL (Schrodinger, 2015). (E) Various PEG molecules are located at the surface of RdRp and mediate interactions with symmetry-related molecules.

dengue RdRp have only been solved in the closed conformation (Noble and Shi, 2012). Interestingly, in the ligand bound structure (PDB ID: 3VWS; Noble et al., 2013) one region involved in ligand binding near motif G has the whole motif present although the overall structure is still in the closed conformation.

Being essential for viral replication and with no equivalent in host cells, DENV RdRp represents an attractive target for drug development. Also, given its structural and conformational conservation among the various serotypes (Rawlinson et al., 2006), the RdRp domain represents one of the most viable targets for the development of direct-acting DENV antivirals. The clinical use of inhibitors against the HBV, HCV and herpes virus polymerase as well as the HIV reverse transcriptase, has validated viral polymerases as therapeutic targets (De Clercq et al., 2006). At present, the only clinically approved antiviral therapy targeting a *Flaviviridae* RdRp is used for the treatment of HCV infections (Bonaventura and Montecucco, 2016; Younossi et al., 2016). The study of antivirals targeting DENV RdRp has led to the identification of a few potential candidates, but further work is needed to develop a viable drug (Noble et al., 2013, 2016; Yokokawa et al., 2016). In order to further advance drug development efforts against the RdRp of DENV and other *Flaviviridae*, determining the structures of the RdRps for rational drug design is of crucial importance.

To date, several RdRp structures of various members of the *Flaviviridae* family have been determined either in the apo

state or in complex with inhibitors or fragments (Noble et al., 2013, 2016). Apo structures of RdRp provide information about structural similarities and differences within the family, which has to be taken into consideration during the various phases of the drug discovery process. In contrast, crystal structures of RdRps in complex with small molecules or fragments provide insights into inhibitor binding pockets for the development of new antivirals.

The commercial screens currently available for crystallization trials require extensive screening for crystals, which is time consuming, cumbersome and expensive. No targeted crystallization screen for viral RdRp proteins is currently available. In order to address these limitations, we have developed a fast and cost-effective RdRp screen with the intent of facilitating crystallization of RdRps from different viruses either alone, or in complex with inhibitors or fragments. Our aim was to rationalize the crystallization processes for different RdRps, by searching the PDB and the literature for crystallization conditions of all known RdRp structures, and to develop a screen specifically designed for crystallization of these proteins. We devised a crystallization screen comprising of 96 different conditions, optimized for use in 96-well plate format. We have further verified these screening conditions by crystallizing the RdRps of DENV serotypes 2 and 3. Furthermore, we obtained RdRp3 in complex with the fragment PC-79-SH52 (Noble et al., 2016) using our novel screen under both soaking and co-crystallization conditions.

2

RESULTS

Data mining and analysis of the PDB

Information about each viral RdRp was retrieved. This included the PDB ID, crystallization method, pH, the crystal growth procedure and conditions, the resolution, and space group for each entry. A crystallization dataset with 201 unique entries was created as shown in Table S1. The RdRp domains deposited in the PDB database originate from 19 different viruses. The most studied virus is HCV, counting 49% of all entries, reflecting the importance of HCV RdRp as therapeutic target of new drugs introduced to the market, followed at a significant distance by Poliovirus (12% of the entries). Other extensively studied viruses are DENV serotype 3, foot and mouth disease virus, and murine norovirus, each representing 5% of the entries (Fig. 2A). The success of specific inhibitors against HCV RdRp underpins the importance of this novel screen for structure-based drug design targeting the RdRp of other viruses of significant public health concern.

To generate the data set, analysis of the crystallization conditions was carried out taking into account the precipitant used, the buffer, as well as its pH, the salt composition and the crystallization temperature (Table S1). Unfortunately, in about 15% of entries, the information deposited in the PDB or in the corresponding manuscript did not include exact crystallization conditions.

A range of temperatures from 273K (0°C) to 303K (30°C) were used to crystallize RdRps. The most used temperatures were 293K (20°C; 28%), 289K (16°C; 24%) and 298K (25°C; 16%). Only very few structures were determined at 277K (4°C) (1%) and above 298K (30°C) (0.5%). For 12% of entries there was no specified crystallization temperature (Fig. 2B).

We observed that the majority of crystals were obtained in a range of pH values between 4.6 and 10.0. Most of the structures were determined at a pH between 7.0–7.5 (29%), and between 4.7–5.0 (28%), followed by pH ranges 6.0–6.6 (25%). The most used single pH values were 7.5 (15%), 7.0 (13%), 4.9 (11.5%) and 5.0 (11%). For 6% of the entries there was no specified pH value (Fig. 2C).

The buffers used to maintain this pH principally included acetate buffer (42%), tris (hydroxymethyl)amino-methane (Tris, 27%), citrate (26%), cacodylate (16%), 2-[4-(2-hydroxyethyl) piperazine-1-yl] ethane-sulfonic acid (HEPES, 14%), 2-(N-morpholino) ethanesulfonic acid (MES, 14%), and Bis-tris propane buffer (11%). Around 3% of entries did not specify the buffer used (Fig. 2D).

The precipitating agent most commonly employed for crystallization was polyethylene glycol (PEG), used in 88% of the cases. A variety of PEGs with different molecular weights were used including PEG 4000 (47%), followed by PEG 550 monomethyl ether (MME, 16%), PEG 8000 and PEG 3350 (both 9%), PEG 400 (7%) and PEG 5000 MME (4%). The second most employed precipitating agent were sulfate salts, in around 23% of the entries, including ammonium sulfate in 9% of the cases, lithium sulfate (11%) and magnesium sulfate (3%) (Fig. 2E).
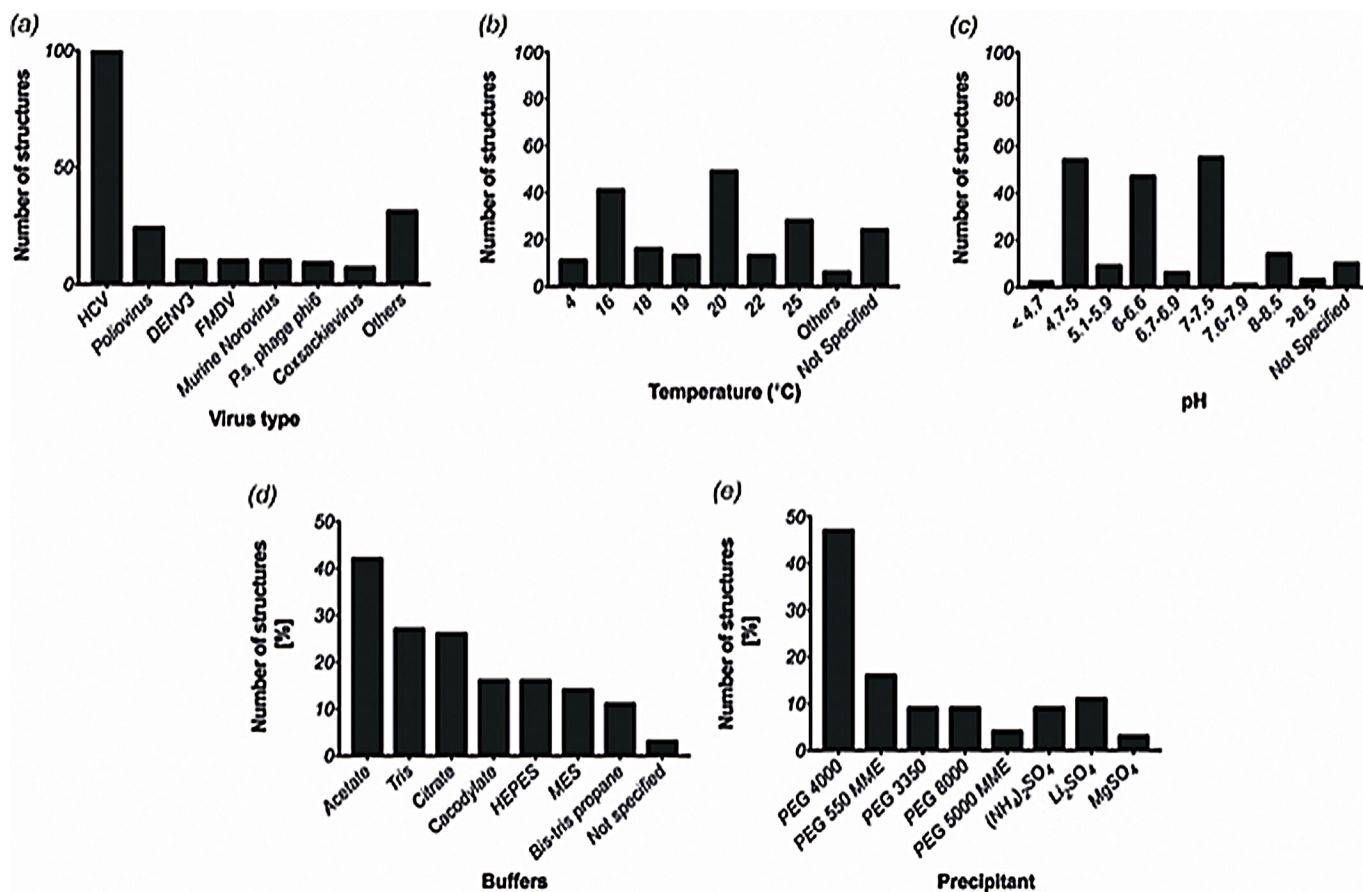
Fig. 2. Analysis of PDB data. (A) Deposited structures of RdRp domains of different viruses. HCV has the highest number of PDB entries (∼100 structures), whereas other major viruses have about 10–20 PDB entries. (B) A range of temperatures have been employed to obtain crystals for RdRp domains with 20°C being the most common one followed by 16°C and room temperature (25°C). Other temperatures have been used sparingly to obtain crystals. (C) Although a wide range of pH values have been successful in obtaining various crystals, pHs closer to physiological pH values have been more successful than others. Bar diagram representation of percentage structures obtained (D) under various buffers and (E) obtained with various precipitating agents from the PDB data analysis.

3

Cations and additives also seemed to be important for the formation of crystals. The most used monovalent cation is Na^+ (51%) from acetate buffer, sodium chloride and Na/K tartrate, followed at some distance by Li^+ (6%) (e.g. lithium sulfate and lithium nitrate) and by K^+ (3%) included in Na/K tartrate, potassium fluoride and potassium phosphate. Divalent cations commonly used are Mg^{2+} (12%) such as magnesium chloride, acetate buffer and magnesium sulfate, and Mn^{2+} (9%) from manganese chloride. Less used is Ca^{2+} (3%) such as in acetate buffer and calcium chloride.

In the case of additives, glycerol was used in 44% of all crystallization conditions, but was also employed as a supplement during protein purifications. This indicates that glycerol was used as an additive to increase protein solubility, to decrease the number of nucleation centres and as a cryo-protectant. Other alcohols such as 2-propanol (6%), ethylene glycol (2%) and 1,6-hexanediol (1%) have been used as additives in the crystallization of various different RdRps.

Design of the RNA polymerase screen

Based on the most successful conditions identified in the PDB analysis, the RNA polymerase screen was designed to include 96 crystallization conditions covering the widest possible variety of precipitants, buffers and pH values, salts and additives. The identified conditions were initially grouped based on the precipitant used and, within each group, ordered by the precipitant concentration. Five different precipitants were selected for the screen. Sparingly used precipitants such as sodium potassium tartrate, ammonium sulfate, etc. were employed to populate the majority of rows A and B of the 96-well screen format. According to the PDB analysis, different concentrations (1–40%) of PEG chains of varying lengths (400–20,000) were most abundantly used to obtain RdRp structures from distinct viruses. Therefore, about 70 of the 96 formulated conditions contain some form of PEG as a precipitant.

Next, we decided to include in the screen a pH distribution between pH 4.7 and pH 10.0, in order to cover the pH range most frequently used in the PDB dataset as extensively as possible. For each individual precipitating agent, we moved from the lowest pH to the highest pH. This trend has been maintained in a serpentine manner with the majority of low pH values towards the lower denomination column and the higher pH values in the higher denomination columns. Few exceptions to this rule are due to space constraints, as we chose to give the screen a larger variation in the use of precipitants rather than the pH. As final criteria, the salt used in each formulation was considered in order to further expand the conditions for the screen. Based on our PDB analysis, the most abundant monovalent and divalent cations that we included in our formulation are Na^+ and Mn^{2+}, respectively. However, we also tried to include the largest number of salts and concentrations possible for each precipitant of the screen. Additives have also been included in some conditions in minute amounts and we placed the same condition with and without additives in adjacent wells. The complete formulation of the RdRp screen is shown in Table 1. The details of well compositions with volumes of each component used are shown in Table S2. The source and stock solutions of each chemical used in the screen are listed in Table S3.

Crystallization results

To validate the RdRp screen developed, we tested whether we could obtain crystals of DENV serotype 3 RdRp. This protein appeared to be a highly promiscuous crystallizer: crystals were obtained in 36 distinct conditions, more than a third of all crystallization conditions provided in our screen. A selection of photos of the crystals is shown in Fig. 3. Most of the crystals grew within 2–4 days to a size sufficient to examine their diffraction potential; however, in order to

obtain larger crystals, crystals obtained from the initial screen in nano-drops were next grown under the same conditions in micro-drops, without further optimization.

The most successful precipitant agent was found to be PEG (in accordance with the PDB analysis), present at an average concentration of 20% in 24 of the 36 conditions that yielded crystals. Specifically, PEG with a chain length of 4000 was most prevalent amongst the successful conditions. The pH range covered by conditions containing PEG varied largely between 4.7 and 8.5, but the majority of the crystals were obtained at pH values of 5.0, 6.5 and 8.0. There appears to be no correlation between the formation of crystals and the buffer used to maintain the pH, with a variety of buffers used in the successful conditions, including Tris, Bis-Tris propane, MES, acetate and citrate buffers. Similarly, salt in the crystallization conditions seemed to have a minimal effect on crystal formation.

Crystals obtained in PEG-containing conditions were observed to be variable in shape and size, with most appearing as single crystals. Thirteen conditions out of the 24 provided high quality data better or equal to 3.0 Å to determine their structures, whereas the remaining crystals either showed no diffraction or diffraction at a much lower resolution not suitable for structure solution (Table S4).

The second most successful precipitant agents for obtaining protein crystals were salts such as, for example, sodium-potassium tartrate, sodium chloride and sodium malonate. All but one yielded resolution of less than 3.0 Å. Four conditions containing ammonium sulfate generated crystals, from one of these we were able to collect diffraction data and solve the structure at 3.0 Å. Others conditions had crystals which were either too small to measure at an X-ray source, or diffracted to a lower resolution needing further optimization. The pH range covered by these conditions was between 6.0–9.5 and was maintained using a variety of buffers [Tris, HEPES, MMT (DL-malic acid, MES and Tris base in the molar ratios 1:2:2) and sodium cacodylate]. Again, crystals obtained under these conditions were single and variable in shape and size. Diffraction details of the crystals obtained are shown in Table S4. In total, we identified 13 different conditions yielding high quality RdRp crystals, which needed no further optimization to obtain the structures. Protein crystals that would have required further optimization of their crystallization conditions were not pursued further.

Diffraction data quality analysis from various screen conditions

A summary of the details of crystals obtained is shown in Fig. 3 and Table S4. Previously published crystallization conditions of dengue RdRp3 are represented in the screen in wells C2 (Ref.: PDB ID 2J7U) and D1 (Ref.: PDB ID 4HHJ), both of which resulted in good diffracting crystals with resolution of 2.3 Å and 2.1 Å, respectively. Interestingly, some of the conditions consistently produced crystals within a high-resolution range. The resolution obtained for these screen conditions are summarized in Fig. 1B.

From the diffraction pattern of the 88 crystals measured at either 12% or 14% glycerol we could conclude that 14% glycerol was optimal for cryoprotection of these crystals. 12% glycerol as a cryoprotectant was not sufficient as it resulted in ice rings (Fig. 1C) for the majority of crystals and also resulted in loss of resolution. We have collected complete datasets using both 12% and 14% glycerol and the quantitative representation of the formation of ice rings at different glycerol concentrations is presented in Fig. 1D.

Data processing and structure determination

Data were processed and reduced using either iMosflm (Battye et al., 2011) or XDS (Kabsch, 2010) and SCALA from the CCP4

4

Table 1. Formulation of RdRp screen

	1	2	3	4	5	6	7	8	9	10	11	12
A	0.05 M MES, pH 5.0 / 3.655 M NaCl / 15% Glycerol	0.05 M MMT, pH 5.5 / 3.655 M NaCl / 15% Glycerol	0.05 M $(CH_3)_2AsO_2Na$, pH 6.5 / 3.655 M NaCl / 15% Glycerol	0.085 M HEPES, pH 7.0 / 3.655 M NaCl / 15% Glycerol	0.085 M Tris, pH 7.5 / 1.275 M $(NH_4)_2SO_4$ / 25% Glycerol	0.05 M Tris, pH 7.5 / 1.29 M $(NH_4)_2SO_4$ / 24.5% Glycerol	0.05 M Tris, pH 7.5 / 1.29 M $(NH_4)_2SO_4$ / 24.5% Glycerol	0.050 M Tris, pH 8.5 / 1.29 M $(NH_4)_2SO_4$ / 24.5% Glycerol	0.05 M SPG, pH 9.0 / 1.29 M $(NH_4)_2SO_4$ / 24.5% Glycerol	0.1 M MES, pH 5.0 / 0.002 M $MnCl_2$ / 0.002 M $MgCl_2$ / 1.3 M $(NH_4)_2SO_4$	0.1 M Bis-Tris, pH 6.1 / 1 mM DTT / 10 mM $NiSO_4$ / 1.3 M $(NH_4)_2SO_4$	0.1 M $(CH_3)2AsO_2Na$, pH 6.5 / 1 M $(NH_4)_2SO_4$
B	0.1 M $(CH_3)2AsO_2Na$, pH 6.5 / 0.2 M NaCl / 2.0 M $(NH_4)_2SO_4$	0.05 M HEPES, pH 7.0 / 0.1 M NaCl / 1.5 M $(NH_4)_2SO_4$ / 2 mM DTT	0.05 M HEPES, pH 7.5 / 0.1 M NaCl / 1.5 M $(NH_4)_2SO_4$ / 2 mM DTT	0.05 M TRIS, pH 8.0 / 1.5 M $(NH_4)_2SO_4$ / 11% glycerol	0.05 M TRIS pH 8.5 / 1.5 M $(NH_4)_2SO_4$ / 11% glycerol	0.1 M CHES, pH 9.5 / 0.2 M NaCl / 1.26 M $(NH_4)_2SO_4$	0.1 M CAPS, pH 10 / 0.2 M Li_2SO4 / 2 M $(NH_4)_2SO_4$	0.1 M MMT, pH 5.0 / 0.8 M K/Na Tartrate	0.1 M MMT, pH 5.5 / 0.8 M K/Na Tartrate, / 0.5% w/v PEG 550 MME	0.1 M MMT, pH 6.0 / 0.8 M K/Na Tartrate	0.1 M $(CH_3)2AsO_2Na$, pH 6.5 / 0.8 M K/Na Tartrate	0.1 M HEPES, pH 7.0 / 0.8 M K/Na Tartrate, / 1% w/v PEG 400
C	0.1 M HEPES, pH 7.5 / 0.8 M K/Na Tartrate	0.1 M Tris, pH 8.5 / 0.8 M K/Na Tartrate / 0.5% PEG 5000 MME	0.1 M Tris, pH 8.5 / 0.8 M K/Na Tartrate, / 1% PEG 2000 MME	0.1 M $(CH_3)2AsO_2Na$, pH 6.5 / 0.125 M NaCl / 1.2 M $Na_3C_6H_5O_7$	0.1 M HEPES, pH 7.5 / 0.01 M NaI / 1.3 M $C_2H_2O_4Na_2$	0.1 M HEPES, pH 7.0 / 2 M $C_2H_3NaO_2$, pH 7.1 / 1% PEG 550 MME	0.1 M $(CH_3)2AsO_2Na$, pH 7.1 / 2 M $C_2H_3NaO_2$	0.05 M MES, pH 5 / 1.0 M NaCl / 20% PEG 400 / 5 mM DTT	0.1 M Bis-Tris propane, pH 6.5 / 0.05 M $(NH_4)_2SO_4$ / 30% PEG550 MME	0.1 M HEPES, pH 7.5 / 0.05 M $MgCl_2$ / 30% PEG550 MME	0.1 M HEPES, pH 7.5 / 0.05 M $MnCl_2$ / 25% PEG 550 MME	0.05 M Tris, pH 7.5 / 0.2 M NH_4OAc 25% PEG 550 MME
D	0.1 M Tris, pH 8.0 / 25% PEG 550 MME	0.1 M Tris, pH 8.0 / 20% PEG 550 MME	0.1 M Tris, pH 8.5 / 20% PEG 550 MME	0.1 M Bicine, pH 9.0 / 25% PEG 550 MME	0.05 M MES, pH 6.5 / 0.2 M $(NH_4)_2SO_4$ / 0.25 M NH_4OAc / 25% PEG 1000	0.1 M MMT, pH 8.0 / 25% PEG 1500	0.1 M MES, pH 6.5 / 20% PEG 2000	0.1 M NH_4OAc, pH 5.0 / 0.2 M $(NH_4)_2SO_4$ / 30% PEG 2000 MME	0.1 M HEPES, pH 7.0 / 1.0 M $C_4H_6O_4$ / 1% PEG 2000 MME	0.1 M $Na_3C_6H_5O_7$, pH 5.5 / 18% PEG 3350 / 14% Glycerol	0.1 M Bis-Tris propane, pH 6.0 / 0.2 M NH_4OAc / 30% PEG 3350	0.1 M MES, pH 6.0 / 0.4 M $LiNO_3$ / 10% PEG 3350
E	0.1 M Bis-tris Propane, pH 7.5 / 0.2 M $Na_3C_6H_5O_7$ / 20% PEG 3350	0.1 M Bis-tris Propane, pH 7.5 / 0.2 M $Na_3C_6H_5O_7$ 20% PEG 3350, / 5% MPD / 5 mM $MnCl_2$, / 20 mM ATP / 10 mM NaOH	0.1 M MMT Buffer pH 8.0 / 0.35 M $LiNO_3$, / 12% PEG 3350	0.1 M $C_2H_3NaO_2$, pH 4.7 / 0.05 M $(NH_4)_2SO_4$ / 20% PEG 4000 / 5 mM DTT	0.05 M $Na_3C_6H_5O_7$, pH 4.9 / 26% PEG 4000 / 7.5% Glycerol	0.05 M MES, pH 5.0 / 5 mM DTT / 20% PEG 4000 / 10% Glycerol	0.05 M MES, pH 5.0 / 20% PEG4000 / 5% Glycerol	0.1 M $Na_3C_6H_5O_7$, pH 5.0 / 20% PEG 4000, 5 mM DTT / 10% Glycerol	0.1 M $C_2H_3NaO_2$, pH 5.0 / 0.3 M NaCl / 18% PEG 4000 / 5 mM β-mercaptoethanol	0.1 M $C_2H_3NaO_2$, pH 5.0 / 0.3 M NaCl / 16% PEG 4000 / 10% Glycerol / 5 mM β-mercaptoethanol	0.1 M $Na_3C_6H_5O_7$, pH 5.6 / 0.2 M NH_4OAc / 33% PEG 4000 / 4% γ-butyrolactone	0.1 M $Na_3C_6H_5O_7$, pH 5.6 / 0.035 M $(NH_4)_2SO_4$ / 40% PEG 4000 / 5% Glycerol / 5 mM DTT
F	0.1 M MES, pH 6.0 / 0.2 M $Mg(Ac)_2$ / 30% PEG 4000 / 4% γ-butyrolactone	0.1 M $C_2H_3NaO_2$, pH 6.0 / 0.3 M NaCl / 14% PEG 4000, / 5 mM β-mercaptoethanol	0.05 M $Na_3C_6H_5O_7$, pH 6.5 / 17% PEG 4000	0.1 M $C_2H_3NaO_2$, pH 6.5 / 0.35 M NH_4OAc / 25% PEG 4000	0.1 M $(CH_3)2AsO_2Na$, pH 6.5 / 0.2 M $Mg(Ac)_2$ / 30% PEG 4000	0.1 M $Na_3C_6H_5O_7$, pH 6.8 / 4% PEG 4000 / 7% Isopropanol	0.1 M $C_2H_3NaO_2$, pH 7.5 / 26% PEG 4000 / 7.5% Glycerol	0.1 M $Na_3C_6H_5O_7$, pH 5.0 / 20% PEG 4000	0.1 M HEPES, pH 7.5 / 20% PEG 4000, 8.5% Isopropanol, / 15% Glycerol	0.1 M HEPES, pH 7.5 / 0.002 M $MnCl_2$ / 20% PEG 4000 / 8.5% Isopropanol / 15% Glycerol	0.1 M Tris, pH 8.0 / 0.002 M $MnCl_2$ / 20% PEG 4000 / 8.5% Isopropanol / 15% Glycerol	0.1 M Tris, pH 8.5 / 0.002 M $MnCl_2$ / 20% PEG 4000 / 8.5% Isopropanol / 15% Glycerol
G	0.1 M Bicine, pH 9.0 / 0.002 M $MnCl_2$ / 20% PEG 4000, / 8.5% Isopropanol, / 15% Glycerol	0.75 M Li_2SO_4 / 12% PEG 8000	0.1 M $C_2H_3NaO_2$, pH 5.0 / 0.2 M $(NH_4)_2SO_4$ / 27% PEG 5000 MME	0.1 M MES, pH 5 / 0.4 M $(NH_4)_2SO_4$ / 21% PEG 5000 MME, 10% Glycerol	0.1 M $Na_3C_6H_5O_7$, pH 5.5 / 8% PEG 8000 / 5% Isopropanol	0.1 M MES, pH 6.0 / 0.01 M $MnCl_2$ / 14% PEG 8000, / 14% Isopropanol / 2.5 mM TCEP	0.1 M $(CH_3)2AsO_2Na$, pH 6.4 / 0.2 M $Mg(CH3COO)_2$ / 15% PEG 8000	0.1 M MES, pH 6.5 / 0.2 M $(NH_4)_2SO_4$ / 25% PEG 5000 MME	0.1 M $Na_3C_6H_5O_7$, pH 6.5 / 5% PEG 8000, / 5% Isopropanol	0.1 M MES-Imidazole pH 6.5 (Morpheus) / 0.02 M $C_4H_6O_5$, 10% PEG 8000, / 20% Ethylene Glycol	0.1 M MES, pH 6.5 / 0.002 M $MnCl_2$ / 10% PEG 8000	0.1 M HEPES pH 7.5 / 10% PEG 8000, 8% Ethylene Glycol
H	0.1 M Tris, pH 7.5 / 0.1% (v/v) Tween-20 / 5 mM $CaCl_2$ 2 mM $MgCl_2$ / 12% PEG 8000, / 0.1 M L-proline 15% Glycerol / 7% (v/v) 1,6-hexanediol	0.05 M Tris, pH 7.5 / 0.2 M $(NH_4)_2SO_4$ / 24% PEG 8000 / 15% Glycerol	0.05 M Tris, pH 7.5 / 0.1 M $(NH_4)_2SO_4$ / 0.02 M $MgSO_4$ / 24% PEG 8000 / 15% Glycerol	0.05 M Tris, pH 8.0 / 0.2 M $(NH_4)_2SO_4$ / 24% PEG 8000 / 15% Glycerol	0.05 M Tris, pH 8.5 / 0.2 M $(NH_4)_2SO_4$ / 24% PEG 8000 / 15% Glycerol	0.1 M Tris, pH 7.5 / 0.075 M NaCl / 10% PEG 10,000	0.1 M Tris, pH 8 / 0.075 M NaCl / 10% PEG 10,000	0.1 M Tris, pH 8.5 / 0.075 M NaCl / 10% PEG 10,000	0.2 M NaH_2PO_4, pH 7.0 / 7% PEG 20,000	0.2 M HEPES, pH 7.5 / 7% PEG 20,000	0.2 M Tris, pH 8.0 / 7% PEG 20,000	0.2 M HEPES, pH 8.5 / 7% PEG 20,000

The screen is designed in a 96-well format that represents the different crystallization conditions extracted from the PDB analysis. The precipitant in the screen forms the most important component with the plate being divided based on various precipitants. The pH and the salts used in the screen take into account all the pH and salts previously used for solving RdRp structures. DTT is unstable and has to be added freshly to the screen, before setting up crystallisation drops.
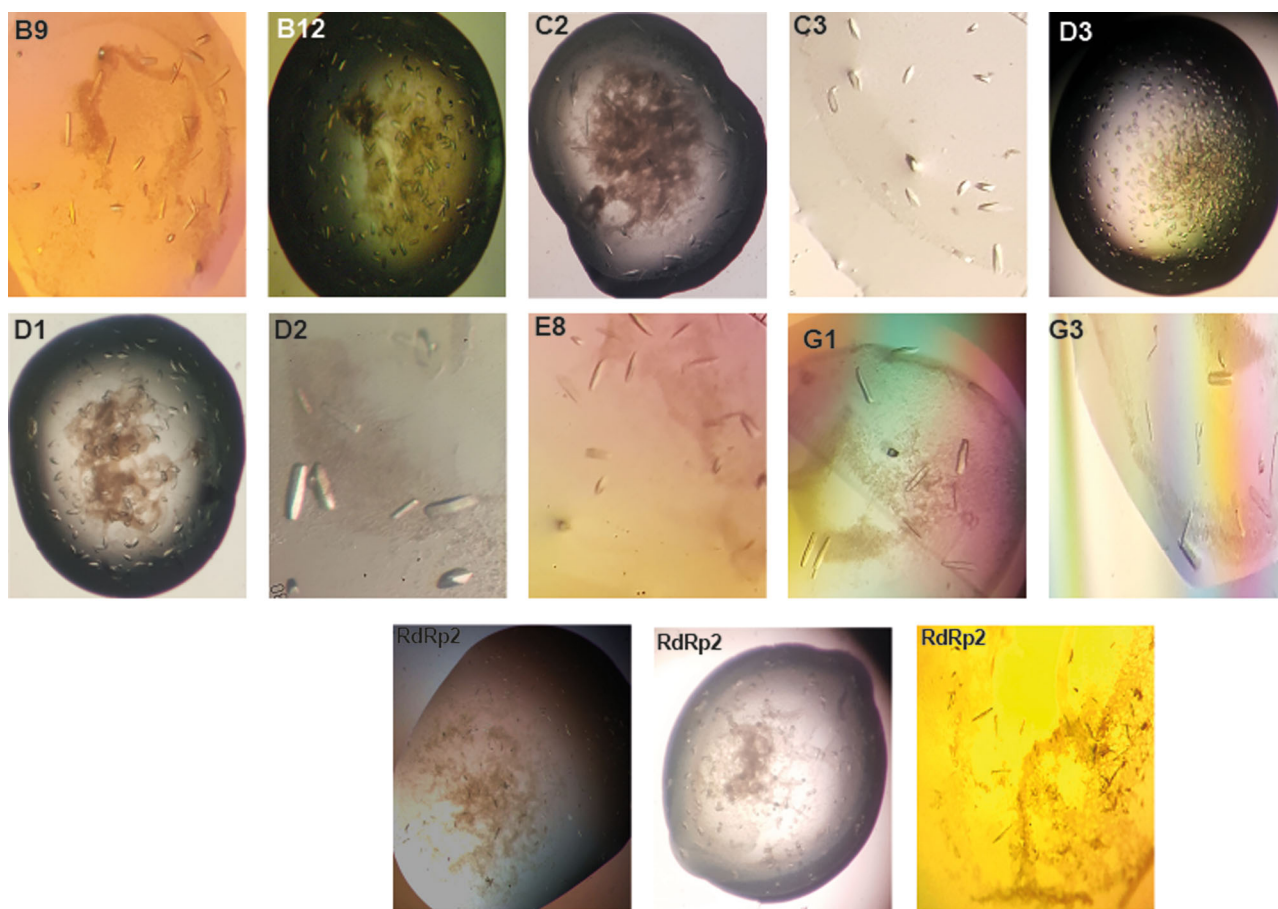
Biology Open

5

Fig. 3. Light micrographs of some of the crystals obtained with the RdRp screen. The images shown represent a selection of crystals obtained directly from the screen, without further optimization of the conditions. The well numbers for each crystal image are displayed at the top left corner. The last panel represents RdRp2 crystals obtained in wells F10, F11 and F12, respectively. Magnifications depicted here may differ among the crystal images. Crystal sizes typically vary from 20–300 µm.

suite of programs (Winn et al., 2011). The structures of dengue RdRp3 were solved by molecular replacement (PHASER MR in CCP4 suite) using the native RdRp3 structure (PDB code 4HHJ, Noble et al., 2013) as a search model. All structures were initially refined with REFMAC5 (Murshudov et al., 1997). Electron density and difference density maps, all σA-weighted, were inspected, and the models were improved using Coot (Emsley and Cowtan, 2004). The refinement of the structures was performed using PHENIX (Adams et al., 2010). The calculation of R_{free} used 5% of data. Crystallographic and refinement statistics are given in Table S5. A list of residues missing in the models and the number of PEG ions as well as water molecules identified are summarized in Table S6.

Surprisingly, all crystals except one crystallize in space group $C222_1$, indicating that the varying crystallization conditions exert no influence on the crystal packing. The architecture of the RdRp structures obtained from the screen adopts the right-hand conformation consisting of fingers, palm and thumb domain (Yap et al., 2007) (Fig. 1A). The structures attain the same closed conformation with loops from motif G (~405–420) and motif F (~450–470) missing in all the structures originating from the screen. All our crystal structures contain two zinc binding pockets represented as blue spheres in the finger and thumb subdomains, respectively (Fig. 1A), which have a tetrahedral coordination geometry as previously described (Yap et al., 2007; Noble et al., 2013).

One structure (PDB ID 2J7U) has one PEG molecule adjacent to Trp823, whereas the second structure (PBD ID 4HHJ) has three PEG entities and one additional P6G (longer ethylene glycol chain) bound to the structure. Twelve of our 13 structures contain PEG molecules but the number of PEGs varies depending on the crystallization condition. We could not establish a relationship between the number of PEG ions present in the structure and the type of PEG used in the crystallization condition. We also could not correlate the number of PEG ions and the resolution of the crystals (Table S5). The role of PEG in the structures is difficult to decipher but the best assumption is that they stabilize the interaction with symmetry-related molecules as most of them are present at the interface of the unit cell and a symmetry related molecule (Fig. 1E).

Overall we conclude that, along with the previous established conditions of dengue RdRp3, we have now found 11 additional conditions, which provide reproducible high-resolution structures without further need for optimization of the crystals. These conditions provide the best diffraction quality crystals with good statistics and therefore can be used for small molecule and fragment crystallization assays. We identified a variety of additional crystallization conditions, but these would require further optimization to obtain structures. Although in this study we obtained a large number of high quality crystals at 18°C, the possibility of using the screen at other temperatures has not been tested for DENV3 RdRp. Until recently there were no crystal structures available for the other serotypes of dengue virus. Recently

a structure of dengue RdRp serotype 2 in complex with a small molecule has been published (Lim et al., 2016). In line with the previously published structure we also obtained crystals for dengue RdRp serotype 2 in various conditions at 4°C; however, these crystals were not single (Fig. 3) and diffracted between 4.0 to 5.0 Å resolution (not shown). Optimization of these conditions is now in progress to obtain single high-quality crystals. Therefore, our RdRp-specific crystallization screen can provide an additional avenue and starting point for the discovery of successful conditions for RdRp proteins or RdRp-ligand complexes.

Description of the structure of the RdRp3-PC-79-SH52 complex obtained by soaking and co-crystallization techniques

The complex structures obtained by co-crystallization (PDB ID: 6H80) and by soaking (PDB ID: 6H9R) are practically identical. They were both obtained using the well condition C1 and C2 from our screen. Both RdRp3 structures lack residues 312–318, 343–354, 406–418, 454–469 and 581–586. The PC-79-SH52 fragment is bound in the palm domain of RdRp protein as previously described (Noble et al., 2016). A significant proportion of the binding is driven by hydrophobic interactions mediated by the thiophene and phenyl ring systems. The sulphur atom of PC-79-SH52 interacts with the side chains of Ala799, Ser796 and Leu511. The thiophene ring points towards the predominantly hydrophobic portion of the inhibitor-binding pocket formed by His711, Met761, Met765, His798 and Trp803. The phenyl moiety also has hydrophobic interactions with Arg729 and Cys709. The carboxyl group forms key hydrogen bonding interactions mediated by water molecules

with main chains atoms of Thr794 and Trp795 (Fig. 4; Fig. S1). Overall, the structure of the RdRp3 in complex with the PC-79-SH52 fragment is similar to the previously published structure (PDB ID: 5F3Z; Noble et al., 2016). Therefore we conclude that our screen will also be suitable for future studies on structure-based drug design targeting RdRps.

DISCUSSION

Certain members of the *Flaviviridae* family are important global pathogens raising significant public health concerns. Their RNA-dependent RNA polymerases represent key targets to treat infections and are intensively studied since there are no mammalian homologues.

The RdRp screen was developed and validated by crystalizing dengue RdRp serotypes 2 and 3, and serotype 3 in complex with a known fragment. PEG molecules of various molecular weights appeared to be the most successful precipitant, in particular PEG 4000. RdRp3 is a promiscuous crystallizer and crystals were obtained in 36 out of 96 distinct conditions, 13 of which did not need any further optimization, yielding crystals diffracting to a high resolution (2.0–3.0 Å). Thirteen complete data sets were collected and structures were obtained from all these data sets.

We believe this study provides a promising platform to screen and crystallize polymerases from other viruses, including emerging RNA viruses such as ZIKV. Studies using the RdRp screen to crystallize the serotypes 1 and 4 of dengue RdRp are underway. Indeed, it will be interesting to observe if optimal crystallization conditions are shared amongst the different serotypes, given their high structural similarity. This screen, which is convenient, fast and
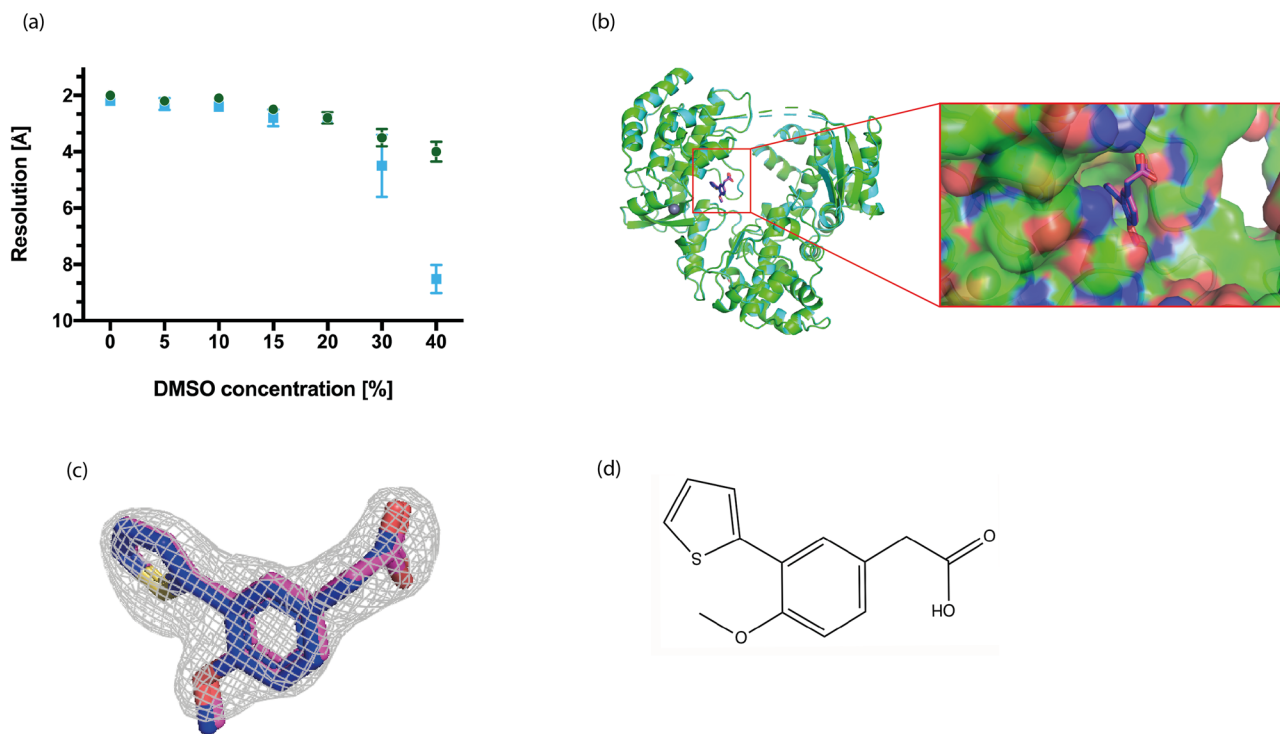
Fig. 4. Structure of RdRp3 in complex with its inhibitor. (A) Graph representing the DMSO concentration plotted against the resolution using native DENV RdRp3 crystals at 1 h (●) and 3 h (■) incubation time (n=12, mean±s.d.). This allowed us to determine the optimal percentage of DMSO and fragment that can be employed for soaking, data collection and subsequent structure determination. (B) Overall superimposition of the structure of the RdRp3 domain in complex with PC-79-SH52 obtained via co-crystallization (green) and soaking (cyan). There are no obvious differences in the two structures or binding conformations of the inhibitor. Magnification of the inhibitor-binding pocket in the Palm domain as a surface with bound PC-79-SH52. (C) The electron-density of the ligand F_o-F_c difference electron density (contoured at 3σ) is shown as a grey mesh with the inhibitor via co-crystallization (blue) and soaking (magenta). (D) Chemical structure of PC-79-SH52.

Table 2. Data collection, structure determination and refinement statistics for the dengue RdRp3-PC-79-SH52 complex[a]

Statistics	Soaking	Co-crystallization
PDB ID	6H9R	6H80
Beamline	I03	I03
Molecules per asymmetric unit	1	1
Resolution range [Å]	48.8–2.4	52.7-2.3
Unit cell parameters [Å, °]	a=164.7, b=181.2, c=57.9, $\alpha=\beta=\gamma=90$	a=165.1, b=181.3, c=57.9, $\alpha=\beta=\gamma=90$
Completeness [%]	99.0 (99.8)	99.8 (99.1)
R_{merge}	5.3 (46.4)	3.2 (48.2)
Multiplicity	2.0 (2.0)	2.0 (2.0)
Mean I/σ(I)	10.6 (2.1)	15.6 (2.0)
CC1/2	99.6 (77.4)	99.9 (80.9)
Total reflections	68,338(6679)	78,203(7695)
Unique reflections	34,409(3371)	39,134(3850)
WILSON B-FACTOR (Å^2)	40.2	49.8
Refinement statistics		
R_{work}/R_{free} [%]	21.3/25.0	21.6/24.8
Average B-factor (Å^2):		
-Overall	51.4	61.9
-RdRp3	51.6	66.2
-Solvent	44.7	53.1
-Ligands	56.2	66.9
No. of PEG/inhibitor/water	8/1/195	5/1/169
r.m.s.d. bond lengths [Å]	0.013	0.013
r.m.s.d. bond angles [°]	1.44	1.45
Ramachandran plot statistics (%):		
-Favoured	95.8	95.8
-Allowed	3.5	3.3
-Outliers	0.7	0.9

[a]Values in parentheses pertain to the highest-resolution shell.

cheap, can be used as a first attempt to crystallize novel RdRps to facilitate an understanding of the fundamental processes underlying the replication of viral genomes.

Importantly, the screen presented in this study can be used for the crystallization of RdRp-ligand complexes and therefore will support structure-based design to develop novel RdRp inhibitors. The crystal structures of RdRp3 in complex with PC-79-SH52 prove how this new crystallization screen can be used for structure-based drug design against RdRps targets. We have obtained nearly identical complex structures using both co-crystallisation of RdRp3 with PC-79-SH52 or soaking native RdRp3 at high concentrations of the fragment. Therefore, our screen is versatile and flexible in using either of the methods for determining future ligand complex structures of RdRps for structure-based drug design. Traditionally, glycerol has been used as a cryo-protectant for diffraction measurements of RdRp crystals. In our case, we optimized the minimum percentage glycerol required for measuring dengue RdRp3 crystals obtained under various conditions in our 96-well screen. The majority of ligands that are used for soaking or co-crystallization experiments are usually dissolved in DMSO. Interestingly, in our soaking experiments we could show that diffraction measurements of RdRp complexes do not require any additional cryo-protectant. Optimization of the tolerance levels of RdRp crystals at increasing DMSO concentrations resulted in 10% DMSO at an incubation time of 1–3 h for optimal experimental conditions (Fig. 4A). This serves two purposes, first the best condition can be used to soak native crystals with high concentrations of inhibitors/fragments in DMSO, without destroying the crystals and thereby increasing the changes of obtaining co-crystal structures for weak binders. Secondly, the soaking, freezing, and data collection pipeline of RdRp crystals is straightforward.

In summary, our screen provided a variety of novel crystallization conditions leading to highly reproducible and high quality RdRp crystals, which are suitable not only for structure-based design, but also for direct crystallization-based fragment screening. In addition, although we did not obtain high quality crystals for RdRp2, optimising the initial crystallisation condition may lead to suitable crystals for structure determination.

MATERIALS AND METHODS

Data mining, analysis of the PDB and the design of the RdRp Screen

The deposited structures of RdRps (alone or in complex with ligands) solved by X-ray crystallography were retrieved and analyzed from the PDB crystallographic database (www.rcsb.org). The details of this database search, which is the basis of this study, are shown in Table S1. The details of the design and development of the screen in 96-well format taking into account all published conditions are shown in Table 1.

Chemistry

The RdRp inhibitor PC-79-SH52 was synthesized as previously described (Noble et al., 2016; Yokokawa et al., 2016).

Cloning, expression and purification of Rdrp3 from dengue virus

DENV RdRp serotype 3 (residues 265–900) was amplified from DENV strain D3/SG/05K/2005, previously subcloned into pcDNA3.1 (kind gift from A. Davidson, University of Bristol) using CloneAmp HiFi PCR Premix (Clontech Laboratories, Inc.) as per the manufacturer's instructions (forward primer: AAGTTCTGTTTCAGGGCCCG.AATGCGGAACCA-GAAACACCC; reverse primer: ATGGTCTAGAAAGCTTTA.CCAAA-TGGCTCCCTCCGACTC). DENV RdRp serotype 2 (residues 266–900) was amplified from DENV strain D2/NGC, previously subcloned into pcDNA3.1 (kind gift from A. Davidson, University of Bristol) using the same procedure as for RdRp serotype 3 (forward primer: AAGTTCTG-TTTCAGGGCCCG.GGAATTGAAAGTGAGATACCA; reverse primer: ATGGTCTAGAAAGCTTTA.CCACAGGACTCCTGCCTCTTC). After purification of the PCR products, the amplified fragments were cloned by recombination into a pOPINF vector, linearized with *KpnI* and *HindIII* restriction enzymes (New England Biolabs), using the In-Fusion® HD Cloning Kit (Clontech Laboratories, Inc.) as per the manufacturer's instructions. DNA sequencing using a T7 primer was used to verify the presence and correct insertion of the constructs.

Escherichia coli BL21(DE3) pLysS cells were transformed with the recombinant plasmid carrying the gene encoding DENV RdRp serotype 3 whereas BL21(DE3) cells were transformed with DENV RdRp serotype 2. Both the proteins were expressed by growing the cells at 37°C in Terrific Broth medium containing 100 mg/l ampicillin until the A$_{600}$ was 0.9–1.2. Protein expression was induced for 22–24 h at 20°C by adding 0.5 mM IPTG (isopropyl-β-D-thiogalactopyranoside). Cells were then harvested by centrifugation at 8000 rpm for 10 min at 4°C and the cell pellets were stored at −80°C.

Cell pellets were resuspended in buffer A (20 mM HEPES, pH 7.5, 500 mM NaCl, 0.01% Tween-20 and 10 mM Imidazole) supplemented with 1 mM PMSF and 2 mg/ml DNase I, lysed by sonication and the lysate was clarified by centrifugation at 20,000 rpm for 1 h 30 min at 4°C.

The supernatant was loaded onto a 5 ml Ni-NTA His-Trap FF crude column (GE Healthcare), pre-equilibrated with buffer A. Unbound proteins were washed away with five column volumes of buffer B containing all components of buffer A, but 30 mM imidazole instead of 10 mM, and the protein was eluted with buffer C (buffer A plus 250 mM Imidazole). Fractions containing the desired protein were detected by using Bradford reagent for qualitative measurement that were later pooled and dialyzed overnight against buffer D (20 mM HEPES, pH 7.5, 0.5 M NaCl, 0.01% Tween-20) together with 3C protease (1 mg of 3C protease for 50 mg of protein) and 3 mM DTT to remove the hexa-histidine tag.

Uncleaved protein and protease were removed by running the sample through a Ni-NTA HisTrap column for a second time. The cleaved protein, which did not bind to the column material, was pooled and the buffer was

8

exchanged with buffer E (50 mM HEPES, pH 7.5 and 0.5 M NaCl). All stages of protein purification were analysed by running samples on SDS-PAGE. The obtained protein was concentrated by ultrafiltration using a Centricon 30 kDa MWCO (Millipore) to reach a final concentration of 10 mg/ml. Finally, the protein was aliquoted in 50 µl aliquots, frozen in liquid nitrogen and stored at −80°C to be used for subsequent crystallization.

The same protocol was followed for DENV RdRp serotype 2 purification, but the following buffers were used: Buffer A1 (50 mM Tris, pH 8.8, 500 mM NaCl, 0.01% Tween-20 and 10 mM Imidazole), buffer B1 (50 mM Tris, pH 8.8, 500 mM NaCl, 0.01% Tween-20 and 30 mM Imidazole), buffer C1 (50 mM Tris, pH 8.8, 500 mM NaCl, 0.01% Tween-20 and 250 mM Imidazole) for affinity purification. Buffer D1 (50 mM Tris, pH 8.8, 0.5 M NaCl, 0.01% Tween-20) was used for overnight dialysis and cleavage with 3C-protease and was buffer-exchanged into buffer E1 (50 mM Tris, pH 8.8 and 0.5 M NaCl) for setting up crystallization trails.

Protein crystallization trials, optimization for diffraction measurements

Crystallization trails were carried using the newly developed RdRp screen with RdRp serotype 3 at 10 mg/ml using a Mosquito Crystal (ttp Labtech) nano-drop robot and 96-well 3-drop Swissci plates (Molecular Dimensions) applying the vapour diffusion sitting drop method.

For the initial screen an equal volume of protein sample and well solution were mixed (100 nl:100 nl). Plates were then incubated at 291K (18°C) for several weeks with regular visual examination. Crystals were obtained in most of the drops within 2–4 days.

Diffraction quality single crystals for each successful condition were obtained using Crystalgen SuperClear™ Plates pre-greased 24-well linbro plates (Jena Biosciences). The drops were set up using 1 µl of protein (10 mg/ml) and 1 µl of well solution using the hanging drop vapour diffusion method.

Crystallization trials for RdRp serotype 2 were set up using the screen by mixing an equal volume of protein sample and well solution (e.g. 100 nl:100 nl). Plates were then incubated at two distinct temperatures at 277K (4°C) and 291K (18°C) for several weeks with regular visual examination. Crystals were obtained in most of the drops within 2–4 days at 18°C and after about 2 weeks at 4°C.

To obtain a co-crystal structure of RdRp serotype 3 in complex with PC-79-SH52 (Noble et al., 2016) using co-crystallization, the protein was incubated with 1 mM of the inhibitor for 1 h at 4°C before setting up crystallization drops.

Determination of inhibitor soaking conditions for optimal diffraction measurements for RdRp serotype 3-inhibitor complexes

The RdRp serotype 3 inhibitor was provided as a 50 mM DMSO stock. For soaking experiments, we initially wanted to obtain the optimal DMSO concentrations and soaking times required without affecting the diffraction quality of our crystals. The graph in Fig. 4A shows how the diffraction quality varies with different DMSO concentrations present in the soaking solutions for different lengths of the soaking time. We determined soaking crystals with compound PC-79-SH52 at 10% DMSO for 1 h to be optimal. To increase our chances in obtaining RdRp3-inhibitor complex via soaking of native crystals with the inhibitor, we tested two different final concentrations of the inhibitor at 20 and 40 mM (maintaining 10% overall DMSO concentration).

For data collection, crystals were frozen in the presence of DMSO, which acted as a cryoprotectant. The crystals were then flash frozen in liquid nitrogen for subsequent measurements using synchrotron radiation.

Data collection, structure determination

Diffraction data for each individual crystal were collected on Massif beamline ID30a-1 at the ESRF and at beamlines I03 and I04 at Diamond Light Source. Data were processed using either XDS (Kabsch, 2010) or iMosflm (Battye et al., 2011) and scaled to resolutions as mentioned in Table S4 (Winn et al., 2011). The structure of the dengue RdRp serotype 3

was solved by molecular replacement. Further details are provided in the section 3.4.2 and the crystallographic statistics are given in Table S5.

References

Adams, P. D., Afonine, P. V., Bunkoczi, G., Chen, V. B., Davis, I. W., Echols, N., Headd, J. J., Hung, L. W., Kapral, G. J., Grosse-Kunstleve, R. W. et al. (2010). PHENIX: a comprehensive Python-based system for macromolecular structure solution. *Acta Crystallogr. D Biol. Crystallogr.* **66**, 213-221.

Aguiar, M., Stollenwerk, N. and Halstead, S. B. (2016). The risks behind Dengvaxia recommendation. *Lancet Infect. Dis.* **16**, 882-883.

Ashour, J., Laurent-Rolle, M., Shi, P. Y. and Garcia-Sastre, A. (2009). NS5 of dengue virus mediates STAT2 binding and degradation. *J. Virol.* **83**, 5408-5418.

Battye, T. G., Kontogiannis, L., Johnson, O., Powell, H. R. and Leslie, A. G. (2011). iMOSFLM: a new graphical interface for diffraction-image processing with MOSFLM. *Acta Crystallogr. D Biol. Crystallogr.* **67**, 271-281.

Bhatt, S., Gething, P. W., Brady, O. J., Messina, J. P., Farlow, A. W., Moyes, C. L., Drake, J. M., Brownstein, J. S., Hoen, A. G., Sankoh, O. et al. (2013). The global distribution and burden of dengue. *Nature* **496**, 504-507.

Bonaventura, A. and Montecucco, F. (2016). Sofosbuvir/velpatasvir: a promising combination. *World J. Hepatol.* **8**, 785-789.

De Clercq, E. and Field, H. J. (2006). Antiviral prodrugs-the development of successful prodrug strategies for antiviral chemotherapy. *Br. J. Pharmacol.* **147**, 1-11.

Dyer, O. (2015). Zika virus spreads across Americas as concerns mount over birth defects. *BMJ* **351**, h6983.

Egloff, M. P., Benarroch, D., Selisko, B., Romette, J. L. and Canard, B. (2002). An RNA cap (nucleoside-2′-O-)-methyltransferase in the flavivirus RNA polymerase NS5: crystal structure and functional characterization. *EMBO J.* **21**, 2757-2768.

Emsley, P. and Cowtan, K. (2004). Coot: model-building tools for molecular graphics. *Acta Crystallogr. D Biol. Crystallogr.* **60**, 2126-2132.

Fields, B. N., Knipe, D. M. and Howley, P. M. (2007). *Fields virology*. Philadelphia: Wolters Kluwer Health/Lippincott Williams & Wilkins.

Iglesias, N. G., Filomatori, C. V. and Gamarnik, A. V. (2011). The F1 motif of dengue virus polymerase NS5 is involved in promoter-dependent RNA synthesis. *J. Virol.* **85**, 5745-5756.

Kabsch, W. (2010). Xds. *Acta Crystallogr. D Biol. Crystallogr.* **66**, 125-132.

Kuno, G., Chang, G. J., Tsuchiya, K. R., Karabatsos, N. and Cropp, C. B. (1998). Phylogeny of the genus Flavivirus. *J. Virol.* **72**, 73-83.

Lim, S. P., Noble, C. G., Seh, C. C., Soh, T. S., El Sahili, A., Chan, G. K., Lescar, J., Arora, R., Benson, T., Nilar, S. et al. (2016). Potent allosteric dengue virus NS5 polymerase inhibitors: mechanism of action and resistance profiling. *PLoS Pathog.* **12**, e1005737.

Lim, S. P., Noble, C. G. and Shi, P.-Y. (2015). The dengue virus NS5 protein as a target for drug discovery. *Antiviral Res.* **119**, 57-67.

Malet, H., Egloff, M. P., Selisko, B., Butcher, R. E., Wright, P. J., Roberts, M., Gruez, A., Sulzenbacher, G., Vonrhein, C., Bricogne, G. et al. (2007). Crystal structure of the RNA polymerase domain of the West Nile virus non-structural protein 5. *J. Biol. Chem.* **282**, 10678-10689.

Malet, H., Masse, N., Selisko, B., Romette, J. L., Alvarez, K., Guillemot, J. C., Tolou, H., Yap, T. L., Vasudevan, S., Lescar, J. et al. (2008). The flavivirus polymerase as a target for drug discovery. *Antiviral Res.* **80**, 23-35.

9

Mazzon, M., Jones, M., Davidson, A., Chain, B. and Jacobs, M. (2009). Dengue virus NS5 inhibits interferon-alpha signaling by blocking signal transducer and activator of transcription 2 phosphorylation. *J. Infect. Dis.* **200**, 1261-1270.

Murshudov, G. N., Vagin, A. A. and Dodson, E. J. (1997). Refinement of macromolecular structures by the maximum-likelihood method. *Acta Crystallogr. D Biol. Crystallogr.* **53**, 240-255.

Noble, C. G., Lim, S. P., Arora, R., Yokokawa, F., Nilar, S., Seh, C. C., Wright, S. K., Benson, T. E., Smith, P. W. and Shi, P. Y. (2016). A conserved pocket in the dengue virus polymerase identified through fragment-based screening. *J. Biol. Chem.* **291**, 8541-8548.

Noble, C. G., Lim, S. P., Chen, Y.-L., Liew, C. W., Yap, L., Lescar, J. and Shi, P.-Y. (2013). Conformational flexibility of the Dengue virus RNA-dependent RNA polymerase revealed by a complex with an inhibitor. *J. Virol.* **87**, 5291-5295.

Noble, C. G. and Shi, P. Y. (2012). Structural biology of dengue virus enzymes: towards rational design of therapeutics. *Antiviral Res.* **96**, 115-126.

Oliveira Melo, A. S., Malinger, G., Ximenes, R., Szejnfeld, P. O., Alves Sampaio, S. and Bispo de Filippis, A. M. (2016). Zika virus intrauterine infection causes fetal brain abnormality and microcephaly: tip of the iceberg? *Ultrasound Obstet. Gynecol.* **47**, 6-7.

Rajapakse, S. (2011). Dengue shock. *J. Emerg. Trauma. Shock.* **4**, 120-127.

Rawlinson, S. M., Pryor, M. J., Wright, P. J. and Jans, D. A. (2006). Dengue virus RNA polymerase NS5: a potential therapeutic target? *Curr. Drug Targets* **7**, 1623-1638.

Ray, D., Shah, A., Tilgner, M., Guo, Y., Zhao, Y., Dong, H., Deas, T. S., Zhou, Y., Li, H. and Shi, P. Y. (2006). West Nile virus 5'-cap structure is formed by sequential guanine N-7 and ribose 2'-O methylations by nonstructural protein 5. *J. Virol.* **80**, 8362-8370.

Schrodinger, L. LC. (2015). The PyMOL Molecular Graphics System, Version 1.8.

Selisko, B., Wang, C., Harris, E. and Canard, B. (2014). Regulation of Flavivirus RNA synthesis and replication. *Curr. Opin. Virol.* **9**, 74-83.

Sousa, R. (1996). Structural and mechanistic relationships between nucleic acid polymerases. *Trends Biochem. Sci.* **21**, 186-190.

Winn, M. D., Ballard, C. C., Cowtan, K. D., Dodson, E. J., Emsley, P., Evans, P. R., Keegan, R. M., Krissinel, E. B., Leslie, A. G., McCoy, A. et al. (2011). Overview of the CCP4 suite and current developments. *Acta Crystallogr. D Biol. Crystallogr.* **67**, 235-242.

Yap, T. L., Xu, T., Chen, Y.-L., Malet, H., Egloff, M.-P., Canard, B., Vasudevan, S. G. and Lescar, J. (2007). Crystal structure of the dengue virus RNA-dependent RNA polymerase catalytic domain at 1.85-Å resolution. *J. Virol.* **81**, 4753-4765.

Yokokawa, F., Nilar, S., Noble, C. G., Lim, S. P., Rao, R., Tania, S., Wang, G., Lee, G., Hunziker, J., Karuna, R. et al. (2016). Discovery of potent non-nucleoside inhibitors of dengue viral RNA-dependent RNA polymerase from a fragment hit using structure-based drug design. *J. Med. Chem.* **59**, 3935-3952.

Younossi, Z. M., Stepanova, M., Feld, J., Zeuzem, S., Jacobson, I., Agarwal, K., Hezode, C., Nader, F., Henry, L. and Hunt, S. (2016). Sofosbuvir/velpatasvir improves patient-reported outcomes in HCV patients: Results from ASTRAL-1 placebo-controlled trial. *J. Hepatol.* **65**, 33-39.

Supporting information

Development and validation of RDRP screen, a crystallization screen for viral RNA-dependent RNA polymerases

Federica Riccio[a1], Sandeep K. Talapatra[a1], Michela Mazzon[b] and Frank Kozielski[a]*

[a]Department of Pharmaceutical and Biological Chemistry, UCL School of Pharmacy, 29-39 Brunswick Square, London, WC1N 1AX, United Kingdom

[b]UCL MRC Laboratory for Molecular Cell Biology, Gower Street, London, WC1E 6BT, United Kingdom

Correspondence email: f.kozielski@ucl.ac.uk; s.talapatra@ucl.ac.uk

[1]Equal Contribution

S1. Summary

Figure S1: The Ligplot of the ligand binding pocket in the palm domain. Dashed green lines indicate hydrogen bonds, and the half-moon represents hydrophobic interactions between residues of the RdRp and compound PC-79-SH52.

Figure S1:

Table S1   Data mining for RdRp crystallization conditions. The details of each RdRp structure submitted to the PDB were individually extracted to design the RdRp screen.

N°	Organism	Protein	PDB Id	Resolution (Å)	Space group	Method & Temperature (°C)	Crystallization condition	PMID & references
1	Bovine viral diarrhea virus	RdRp	2CJQ	2.60	P3$_1$	Sitting drop	10% PEG 8000 0.1 M HEPES, pH 7.5 8% Ethylene Glycol	(Choi *et al.*, 2006)
2	Coxsackievirus	B3 Polymerase F232L mutant	4WFX	1.81	P4$_3$2$_1$2	(16°C)	0.085 M HEPES, 3.655 M NaCl, 15% Glycerol	(Campagnola *et al.*, 2015)
3	Coxsackievirus	B3 Polymerase F232L mutant	4WFY	2.06	P4$_3$2$_1$2	(16°C)	0.085 M Tris, pH 7.5, 1.275 M (NH$_4$)$_2$SO$_4$, 25% Glycerol	
4	Coxsackievirus	B3 3D pol RdRp	4WFZ	1.80	P4$_3$2$_1$2	(16°C)	0.085 M HEPES, pH 7.5 3.6 M NaCl, 15% Glycerol	
5	Coxsackievirus	B3 3D pol with GPC-N114 inhibitor	4Y2A	2.90	P4$_3$2$_1$2	Sitting drop (20°C)	50 mM Tris, pH 7.5 24.5% Glycerol 1.29 M (NH$_4$)$_2$SO$_4$	(van der Linden *et al.*, 2015)
6	Coxsackievirus	B3 3D pol in	4Y34	2.70	P4$_3$2$_1$2	Sitting drop (20°C)	50 mM Tris pH 7.5	

		complex with GPC-N143					24.5% Glycerol 1.2 9 M $(NH_4)_2SO_4$	
7	Coxsackievirus	B3 RdRp (3D pol) with pyrophosphate	3CDU	2.10	$P4_32_12$	Hanging drop (20°C)	2 M $(NH_4)_2SO_4$, 0.1 M CAPS, pH 10.0, 0.2 M Li_2SO_4	(Gruez *et al.*, 2008)
8	Coxsackievirus	B3 RdRp (3D pol) with protein primer VPg and a pyrophosphate	3CDW	2.50	$P4_32_12$	Hanging drop (20°C)	2 M $(NH_4)_2SO_4$, 0.1 M CAPS, pH 10.0 0.2 M Li_2SO_4	
9	Dengue virus serotype 3	NS5 RdRp	2J7U	1.85	$C222_1$	Hanging drop (4°C)	0.1 M Tris-HCl, pH 8.5 0.8 M K/Na Tartrate 0.5% PEG 5000 MME	(Yap *et al.*, 2007)
10	Dengue virus serotype 3	NS5 RdRp complexed with 3'DGTP	2J7W	2.60	$C222_1$	Hanging drop (4°C)	0.1 M Tris-HCl, pH 8.5 0.8 M K/Na Tartrate, 0.5% PEG 5000 MME	
11	Dengue virus serotype 3	RdRp	4HHJ	1.79	$C222_1$	Hanging drop (18°C)	0.1 M Tris, pH 8.0 25% PEG 550 MME	(Noble *et al.*, 2013)
12	Dengue virus serotype 3	RdRp bound to NITD-107	3VWS	2.10	$C222_1$	Hanging drop (18°C)	20% PEG 550 MME 0.1 M Tris pH 8.0	

13	Dengue virus serotype 3	RdRp with residues from the NS5 linker region	4C11	2.60	$P2_12_12$	Sitting drop (20°C)	1.0 M Succinic Acid, 0.1 M HEPES, pH 7.0 1% PEG 2000 MME	(Lim *et al.*, 2013)
14	Dengue virus serotype 3	RdRp bound to PC-79-SH52	5F3Z	2.00	$C222_1$	Hanging drop (18°C)	0.1 M Tris, pH 8.0 25% PEG 550 MME	(Noble *et al.*, 2016)
15	Dengue virus serotype 3	RdRp bound to FD-83-ki26	5F41	2.00	$C222_1$	Hanging drop (18°C)		
16	Dengue virus serotype 3	RdRp bound to JF-31-MG46	5F3T	2.05	$C222_1$	Hanging drop (18°C)		
17	Dengue virus serotype 3	NS5 full length with SAH	4V0Q	2.30	$P2_12_12$	Sitting drop (20°C)	0.2 M $CaAc_2$ or $MgAc_2$ 0.1 M Na Cacodylate, pH 6.4 10-20% PEG 8000	(Zhao *et al.*, 2015)
18	Dengue virus serotype 3	NS5 full length with GTP and SAH	4V0R	2.40	$P2_12_12$	Sitting drop (18°C)	0.1 M Na Cacodylate, pH 6.4 0.2 M $MgAc_2$ or $CaAc_2$ 14% PEG 8000	
19	Enterovirus 71	RdRp	3N6L	2.60	$P3_22_1$	Hanging drop (18°C)	1.3 M $(NH_4)_2SO_4$	(Wu *et al.*, 2010)
20	Enterovirus 71	RdRp	3N6M	2.50	$P3_22_1$	Hanging drop (18°C)	1 mM DTT	

21	Enterovirus 71	RdRp	3N6N	2.90	$P3_221$	Hanging drop (18°C)	0.1 M Bis-Tris pH 6.1 10 mM $NiCl_2$	
22	Foot and mouth disease virus	RdRp K18E mutant with RNA	4WZM	2.57	$P3_221$	Hanging drop (20°C)	30% PEG 4000 0.2 M $MgAc_2$, 0.1 M MES pH 6.0 4% γ-butyrolactone	(Ferrer-Orta *et al.*, 2015)
23	Foot and mouth disease virus	3D pol K18E mutant	4WYL	2.00	$P4_12_12$	Hanging drop (20°C)		
24	Foot and mouth disease virus	3D pol K20E mutant	4WYW	1.80	$P4_12_12$	Hanging drop (20°C)		
25	Foot and mouth disease virus	RdRp K20E mutant with RNA	4WZQ	2.80	$P3_221$	Hanging drop (20°C)	30% PEG 4000 0.2 M $MgAc_2$ 0.1 M MES pH 6.0	
26	Foot and mouth disease virus	RdRp K20A mutant with an RNA	4X2B	2.94	$P4_12_12$	Hanging drop (20°C)		
27	Foot and mouth disease virus	RdRp with a template-primer RNA and ribavirin	2E9R	2.81	$P3_221$	Hanging drop (20°C)	30% PEG 4000 0.2 M $MgAc_2$ 0.1 M Na Cacodylate pH 6.0	(Ferrer-Orta *et al.*, 2007)
28	Foot and mouth disease virus	RdRp with a template-	2E9T	2.60	$P3_221$	Hanging drop (20°C)		

	primer RNA and ATP						
29	Foot and mouth disease virus	RdRp with a template-primer RNA and 5F-UTP	2EC0	2.70	P3$_2$2$_1$	Hanging drop (20°C)	33% NH$_4$Ac 0.1 M Na Citrate pH 5.6 4% butyrolactone	
30	Foot and mouth disease virus	RdRp with uridylylated VPg protein	2F8E	2.90	P3$_2$2$_1$	Hanging drop (20°C)	33% PEG 4000 0.2 M NH$_4$Ac 0.1 M Na Citrate, pH 5.6	(Ferrer-Orta *et al.*, 2006)
31	Foot and mouth disease virus	RdRp with VPg protein	2D7S	3.00	P3$_2$2$_1$	Hanging drop (20°C)	4% Butyrolactone	
32	Hepatitis C virus	NS5B RdRp	1C2P	1.90	P2$_1$2$_1$2$_1$	Batch (22°C)	10% PEG 4000, 10% Glycerol, 5 mM DTT, 5 mM Tris, pH 7.5, 25 mM MES, pH 5.0	(Lesburg *et al.*, 1999)
33	Hepatitis C virus	RdRp	1CSJ	2.80	P2$_1$2$_1$2$_1$	Hanging drop (4°C)	5% PEG 8000, 5% 2-propanol 0.1 M Na Citrate, pH 6.5	
34	Hepatitis C virus	RNA pol in complex with GTP and Mn^{2+}	1GX5	1.70	P2$_1$2$_1$2$_1$	Hanging drop (4°C)	4% PEG 4000 7% 2-Propanol 0.1 M Na Citrate, pH 6.8	(Bressanelli *et al.*, 2002)
35	Hepatitis C virus	RNA pol in complex with	1GX6	1.85	P2$_1$2$_1$2$_1$	Hanging drop (4°C)		

36	Hepatitis C virus	RNA pol with non-nucleoside analogue inhibitor	1NHU	2.00	P2$_1$2$_1$2$_1$	Hanging drop (22°C)	18% PEG 4000 0.3 M NaCl 0.1 M NaOAc, pH 5.0, 0 5 mM 2-mercaptoethanol	(Wang *et al.*, 2003)
37	Hepatitis C virus	RNA pol with NNI	1NHV	2.90	P2$_1$2$_1$2$_1$	Hanging drop (22°C)		
38	Hepatitis C virus	NS5B RNA pol with non-competitive inhibitor	1OS5	2.20	P4$_1$2$_1$2	Hanging drop (20°C)	0.2 M NH$_4$Ac, pH 4.6 30% PEG MME 2000	(Love *et al.*, 2003)
39	Hepatitis C virus	RdRp	1QUV	2.50	P4$_3$2$_1$2	Hanging drop (22.5°C)	21 – 28% PEG 4000, 0.2 -0.35 M NaOAc, 0.1M NH$_4$Ac 0.02 M TES, pH 6.0	(Ago *et al.*, 1999)
40	Hepatitis C virus	NS5b RNA Pol with a covalent inhibitor	2AWZ	2.15	P2$_1$2$_1$2$_1$	Hanging drop (20°C)	200 mM (NH$_4$)$_2$SO$_4$ 27% PEG 5000 MME 100 mM NaOAc, pH 5.0	(Powers *et al.*, 2006)
41	Hepatitis C virus	NS5b Pol with a covalent	2AX1	2.10	P2$_1$2$_1$2$_1$	Hanging drop (20°C)		

Note: the top of the table continues from a previous page with "UTP and Mn^{2+}"

		inhibitor						
42	Hepatitis C virus	Pol with an allosteric inhibitor	2BRK	2.30	$P2_12_12$	Hanging drop (4°C)	5% PEG 8000	(Di Marco *et al.*, 2005)
							5% 2-propanol	
43	Hepatitis C virus	Pol with an allosteric inhibitor	2BRL	2.30	$P2_12_12$	Hanging drop (4°C)	0.1 M Na Citrate, pH 6.5	
44	Hepatitis C virus	NS5B pol with a tetracyclic inhibitor	2DXS	2.20	P_12_1	Hanging drop (4°C)	0.1 M Citrate, pH 5.5 8% PEG 8000 5% 2-propanol	(Ikegashira *et al.*, 2006)
45	Hepatitis C virus	NS5B RdRp with NNI-2 inhibitor	2GIQ	1.65	$P2_12_12_1$	Hanging drop (20°C)	50 mM Na Citrate pH 4.9 26% PEG 4000 7.5% Glycerol	(Le Pogam *et al.*, 2006)
46	Hepatitis C virus	NS5B RdRp with NNI-1 inhibitor	2GIR	1.90	$P2_12_12_1$	Hanging drop (20°C)		
47	Hepatitis C virus	NS5B pol with dihydropyrone -containing inhibitor	2HAI	1.58	$P4_12_12$	Hanging drop (20°C)	30% PEG MME 2000, 0.2 M $(NH_4)_2SO_4$ 0.1 M NH_4Ac, pH 5.0	(Li *et al.*, 2006)
48	Hepatitis C virus	NS5B pol with Thiazolones	2I1R	2.20	$P2_12_12_1$	Evaporation (22°C)	20% PEG 400 5 mM DTT	(Yan, Larson*, et al.*, 2007)

		inhibitor					0.5 M MES, pH 5.0	
							1.0 M NaCl	
49	Hepatitis C virus	NS5B polymerase	2IJN	2.20	P2$_1$2$_1$2$_1$	Evaporation (22°C)	20% PEG 4000	(Yan, Appleby, Gunic, *et al.*, 2007)
							5 mM DTT	
							0.5 M MES, pH 5.0	
							1.0 M NaCl	
50	Hepatitis C virus	NS5B with allosteric inhibitor	2HWH	2.30	P2$_1$2$_1$2$_1$	Evaporation (22°C)	20% PEG 4000	(Yan *et al.*, 2006)
							5 mM DTT	
							0.5 M MES, pH 5.0	
51	Hepatisis C virus	NS5B with allosteric inhibitor	2HWI	2.00	P2$_1$2$_1$2$_1$	Evaporation (22°C)	1.0 M NaCl	
52	Hepatisis C virus	Polymerase with inhibitor SB655264	2JC0	2.00	P2$_1$2$_1$2$_1$		20% PEG 4000,	
							5 mM DTT,	(Slater *et al.*, 2007)
							10% Glycerol	
53	Hepatisis C virus	Polymerase with inhibitor SB698223	2JC1	2.00	P2$_1$2$_1$2$_1$		0.1 M Citrate buffer, pH 5.0	
54	Hepatisis C virus	NS5B pol with Thiazolone-acylsulfonamides allosteric	2O5D	2.20	P2$_1$2$_1$2$_1$	Evaporation (22°C)	20% PEG 4000	(Yan, Appleby, Larson, *et al.*, 2007)
							5 mM DTT	
							0.5 M MES, pH 5.0	

		inhibitors					1.0 M NaCl	
55	Hepatitis C virus – H77	NS5B apo polymerase	2XI2	1.80	P 2_1	Sitting drop	0.1 mM MES, pH 6.5 0.2 M $(NH_4)_2SO_4$ PEG 5000 MME	(Harrus *et al.*, 2010)
56	Hepatitis C virus – H77	NS5B polymerase with GTP	2XI3	1.70	P1	Sitting drop	0.05 M MES, pH 6.5, 0.2 M $(NH_4)_2SO_4$ 0.25 M NH_4Ac 25%-30% PEG 1000	
57	Hepatitis C virus	NS5B pol with Thienopyrrole -based finger-loop inhibitors	2WCX	2.00	$P2_12_12$		0.1 M MES, pH 6.0 14% PEG 8000 14% 2-propanol 10 mM DTT, 10 mM $MnCl_2$	(Martin Hernando *et al.*, 2009)
58	Hepatitis C virus genotype 1B	NS5B pol with a NNI	2WHO	2.00	$P2_12_12_1$		0.1 M MES, pH 6.0 14% PEG 8000 14% 2-propanol 10 mM DTT 10 mM $MnCl_2$	(Ontoria *et al.*, 2009)
59	Hepatitis C virus	NS5B pol with an allosteric	2WRM	1.95	$P2_12_12$		pH 6.0	To be published

		inhibitor of thumb domain					
60	Hepatitis C virus	NS5B pol with a potent non-nucleoside finger-loop inhibitor	2XWY	2.53	P2$_1$2$_1$2		0.1 M MES, pH 6.0 14% PEG 8000 2.5 mM TCEP 14% 2- propanol 10 mM MnCl$_2$	(Narjes *et al.*, 2011)
61	Hepatitis C virus	NS5B polymerase	2ZKU	1.95	P2$_1$2$_1$2$_1$	Hanging drop (25°C)	5 mM 2- Mercaptoethanol 18% PEG 4000 0.3 M NaCl 0.1 M NaOAc, pH 5.0	
62	Hepatitis C virus strain JFH1	NS5B polymerase	3I5K	1.90	P2$_1$	Hanging drop (20°C)	6 to 7% PEG 20000 0.2 M NaH$_2$PO4, pH 7.0	(Simister *et al.*, 2009)
63	Hepatitis C virus	NS5B pol with a novel Pyridazinone inhibitor	3BR9	2.30	P2$_1$2$_1$2$_1$	Hanging drop (25°C)	20% PEG 4000 5 mM DTT 50 mM (NH$_4$)$_2$SO$_4$	(Zhou *et al.*, 2008)
64	Hepatitis C virus	NS5B pol with a novel Pyridazinone	3BSA	2.30	P2$_1$2$_1$2$_1$	Hanging drop (25°C)	0.1 M NaOAc, pH 7.4	

		inhibitor						
65	Hepatitis C virus	NS5B pol with a novel Pyridazinone inhibitor	3BSC	2.65	$P2_12_12_1$	Hanging drop (25°C)		
66	Hepatitis C virus	NS5B pol with a novel Pyridazinone inhibitor	3CDE	2.10	$P2_12_12_1$	Hanging drop (25°C)	20% PEG 4000 5 mM DTT 50 mM $(NH_4)_2SO_4$ 0.1 M NaOAc	(Li *et al.*, 2008)
67	Hepatitis C virus	NS5B RdRp with small molecule fragments	3CIZ	1.87	$P2_12_12_1$	Hanging drop (19°C)	8-11% Glycerol 20-24% PEG 4000 50 mM Na Citrate, pH 4.9	(Antonysamy *et al.*, 2008)
68	Hepatitis C virus	NS5B RdRp with small molecule fragments	3CJ0	1.90	$P2_12_12_1$	(19°C)		
69	Hepatitis C virus	NS5B RdRp with small molecule fragments	3CJ2	1.75	$P2_1$	(19°C)		
70	Hepatitis C virus	NS5B RdRp	3CJ3	1.87	$P2_12_12_1$	(19°C)		

		with small molecule fragments						
71	Hepatitis C virus	NS5B RdRp with small molecule fragments	3CJ4	2.07	$P2_1$	(19°C)		
72	Hepatitis C virus	NS5B RdRp with small molecule fragments	3CJ5	1.92	$P2_12_12_1$	(19°C)		
73	Hepatitis C virus	NS5B pol with a novel Pyridazinone inhibitor	3CO9	2.10	$P2_12_12_1$	(25°C)	20% PEG 4000 5 mM DTT 50 mM $(NH_4)_2SO_4$ 0.1 M NaOAc, pH 4.7	(Ruebsam et al., 2008)
74	Hepatitis C virus	NS5B pol with a novel Pyridazinone inhibitor	3CVK	2.31	$P2_12_12_1$	Hanging drop (25°C)	20% PEG 4000 5 mM DTT 50 mM $(NH_4)_2SO_4$ 0.1 M NaOAc, pH 4.7	(Ellis et al., 2008)
75	Hepatitis C virus	NS5B pol with a novel Pyridazinone	3CWJ	2.40	$P2_12_12_1$	Hanging drop (25°C)	20% PEG 4000 5 mM DTT	(Ellis et al., 2008)

		inhibitor					50 mM $(NH_4)_2SO_4$	
							0.1 M NaOAc, pH 4.7	
76	Hepatitis C virus	NS5B pol with a novel Benziothiazole inhibitor	3D28	2.30	$P2_12_12_1$	Hanging drop (25°C)	20% PEG 4000	(Kim *et al.*, 2008)
							5 mM DTT	
							50 mM $(NH_4)_2SO_4$	
77	Hepatitis C virus	NS5B pol with a novel Pyridazinone inhibitor	3D5M	2.20	$P2_12_12_1$	Hanging drop (25°C)	0.1 M NaOAc, pH 4.7	
78	Hepatitis C virus	NS5B pol with a novel Pyridazinone inhibitor	3E51	1.90	$P2_12_12_1$	Hanging drop (25°C)	20% PEG 4000	(Dragovich *et al.*, 2008)
							5 mM DTT	
							50 mM $(NH_4)_2SO_4$	
							0.1 M NaOAc, pH 4.7	
79	Hepatitis C virus	NS5B pol with 796 inhibitor	3FQK	2.20	$P2_12_12_1$	Hanging drop (20°C)	50 mM Na Citrate, pH 4.9	(Hang *et al.*, 2009)
							7.5% Glycerol	
							24% PEG 4000	
80	Hepatitis C virus	NS5B pol with 796 inhibitor	3FQL	1.80	$P2_12_12_1$	Sitting drop (20°C)	50 mM Na Citrate pH 4.9	
							7.5% Glycerol	
							26% PEG 4000	

81	Hepatitis C virus	NS5B RNA pol with PF868554	3FRZ	1.86	P4$_1$2$_1$2	Hanging drop (25°C)	18.0% PEG 3000 14% Glycerol 0.1 M Citrate, pH 5.5	(Li *et al.*, 2009)
82	Hepatitis C virus	NS5B pol with thiazine inhibitor	3G86	2.20	P2$_1$2$_1$2$_1$	Sitting drop	50 mM Na Citrate pH 4.9 7.5% Glycerol 24% PEG 4000	(de Vicente *et al.*, 2009)
83	Hepatitis C virus	NS5B pol with a monocyclic dihydro-pyridinone inhibitor	3GYN	2.15	P2$_1$2$_1$2$_1$	Hanging drop (25°C)	20% PEG 4000 5 mM DTT 50 mM (NH$_4$)$_2$SO$_4$ 0.1 M NaOAc, pH 4.7	(Ellis *et al.*, 2009)
84	Hepatitis C virus	NS5B pol with a monocyclic dihydro-pyridinone inhibitor	3IGV	2.60	P2$_1$2$_1$2$_1$	Hanging drop (25°C)		
85	Hepatitis C virus	NS5B pol with a bicyclic dihydro-pyridinone inhibitor	3H2L	1.90	P2$_1$2$_1$2$_1$	Hanging drop (25°C)	20% PEG 4000 5 mM DTT 50 mM (NH$_4$)$_2$SO$_4$ 0.1 M NaOAc, pH 4.7	(Ruebsam *et al.*, 2009)
86	Hepatitis C virus	NS5B pol	3H59	2.10	P2$_1$2$_1$2$_1$	Hanging drop (20°C)	50 mM Na Citrate pH 4.9	

		thiazine inhibitor 2				26% PEG 4000 7.5% Glycerol	(de Vicente, *et al.*, 2009)
87	Hepatitis C virus	NS5B pol with saccharin inhibitor	3H5S	2.00	P2$_1$2$_1$2$_1$	Sitting drop (20°C)	50 mM Na Citrate, pH 4.9 26% PEG 4000 7.5% Glycerol	
88	Hepatitis C virus	NS5B pol with saccharin inhibitor 1	3H5U	1.95	P2$_1$2$_1$2$_1$	Sitting drop (20°C)	50 mM Na Citrate, pH 4.9 24% PEG 3350 7.5% Glycerol	
89	Hepatitis C virus	NS5b 1b with a pyrimidine derivative	3H398	1.90	P2$_1$2$_1$2$_1$	Sitting drop (20°C)	12-17.5% PEG 4000 8-11% Glycerol 0.1 M Na Citrate, pH 4.5-6.0	(Wang *et al.*, 2009)
90	Hepatitis C virus	NS5B pol with thumb site inhibitor	3MF5	2.00	P2$_1$2$_1$2$_1$	Sitting drop (0°C)	26% PEG 4000 7.5% Glycerol 50 mM Na Citrate, pH 4.9	(Yang *et al.*, 2010)
91	Hepatitis C virus	NS5B pol with 3-heterocyclic quinolone	3UDL	2.15	P2$_1$2$_1$2$_1$	(18°C)	16% PEG 4000 10% Glycerol 0.3 M NaCl 5 mM ß-mercaptoethanol 0.1 M NaOAc, pH 5.1	(Kumar *et al.*, 2011)

92	Hepatitis C virus	NS5B RNA pol with a piperazine inhibitor	3QVS	1.90	$P2_12_12_1$	Hanging drop (10°C)	0.1 M NaOAc, pH 6.0 14% PEG 4000 0.3 M NaCl 5 mM 2-mercaptoehanol 2.4 mM n-octanoylsucrose	(Ando *et al.*, 2012)
93	Hepatitis C virus	NS5B genotype 2A JFH-1 with primer-template RNA	4E7A	3.00	$P6_5$	Sitting drop (16°C)	30% PEG 3350 0.1 M Bis-Tris propane, pH 6.0 0.2 M NH_4Ac	(Mosley *et al.*, 2012)
94	Hepatitis C virus	NS5B genotype 2A JFH-1 with primer template RNA	4E78	2.50	$P6_5$	Sitting drop (16°C)		
95	Hepatitis C virus	NS5B genotype 2A JFH-1 with beta hairpin loop deletion	4E76	2.90	$P6_5$	Sitting drop (16°C)	30% PEG 550 MME 0.1 M Bis-Tris propane, pH 6.5 50 mM $(NH_4)_2SO_4$	
96	Hepatitis C virus	NS5B pol inhibited by Tri-substituted	4EO6	1.79	$P2_12_12_1$	Sitting drop (20°C)	15-20% PEG 4000 10% Glycerol,	(Canales *et al.*, 2012)

		acylhydrazines					0.1 M NaOAc, pH 4.8-5.0	
97	Hepatitis C virus	NS5B pol inhibited by Tri-substituted acylhydrazines	4EO8	1.80	P2$_1$2$_1$2$_1$	Sitting drop (20°C)		
98	Hepatitis C virus	NS5B (BK)pol with fragment-based compounds	4IH5	1.90	P2$_1$2$_1$2$_1$	Sitting drop (25°C)	26% PEG 4000 7.5% Glycerol 50 mM Na Citrate, pH 4.9	(Talamas *et al.*, 2013)
99	Hepatitis C virus	NS5B (BK)pol with fragment-based compounds	4IH6	2.20	P2$_1$	Sitting drop (20°C)		
100	Hepatitis C virus	NS5B (BK)pol with fragment-based compounds	4IH7	2.30	P2$_1$2$_1$2$_1$	Sitting drop (25°C)		
101	Hepatitis C virus	NS5B GT1B N316 with GSK5852A	4KAI	2.19	P2$_1$2$_1$2$_1$	Sitting drop (25°C)	0.1 M Na-citrate pH 5.0 17% PEG 4000	(Maynard *et al.*, 2014)

102	Hepatitis C virus	NS5B GT1B N316Y with CMPD 32	4KB7	1.81	$P2_12_12_1$	Sitting drop (25°C)	10% Glycerol	
103	Hepatitis C virus	NS5B GT1B N316Y with CMPD 4	4KBI	2.06	$P2_12_12_1$	Sitting drop (25°C)		
104	Hepatitis C virus	NS5B GT1B N316Y with GSK5852	4KE5	2.10	$P2_12_12_1$	Sitting drop (25°C)		
105	Hepatitis C virus	NS5B 1b (BK) with RG7109	4MIA	2.80	$P2_12_12_1$	Sitting drop (19°C)	24% PEG 4000 7.5% Glycerol 50 mM Na Citrate, pH 4.6	(Talamas et al., 2014)
106	Hepatitis C virus	NS5B 1b (BK) with Compound 48	4MIB	2.30	$P2_12_12_1$	Sitting drop (19°C)	26% PEG 4000 7.5% Glycerol 50 mM Na Citrate, pH 4.9	
107	Hepatitis C virus	NS5B 1b (BK) with inhibitor 2	4MK7	2.80	$P2_12_12_1$	Sitting drop (19°C)	26% PEG 4000 7.5% Glycerol 50 mM Na Citrate, pH 4.9	(Schoenfeld et al., 2013)
108	Hepatitis C virus	NS5B 1b (BK) with inhibitor 4	4MK8	2.09	$P2_12_12_1$	Sitting drop (19°C)		

109	Hepatitis C virus	NS5B 1b (BK) with inhibitor 14	4MKB	1.90	$P2_12_12_1$	Sitting drop (19°C)		
110	Hepatitis C virus	NS5B 1b (BK) with inhibitor 12	4MK9	2.05	$P2_12_12_1$	Sitting drop (19°C)	26% PEG 4000 7.5% Glycerol 50 mM Tris, pH 7.5	
111	Hepatitis C virus	NS5B 1b (BK) with inhibitor 13	4MKA	2.05	$P2_12_12_1$	Sitting drop (19°C)		
112	Hepatitis C virus	NS5B 2A with S15G, C223H, V321I mutations	4OBC	2.50	$P6_5$	Sitting drop (16°C)	PACT screen condition D5: 25% PEG 1500 0.1 M MMT buffer, pH 8.0	(Lam *et al.*, 2014)
113	Hepatitis C virus – J6	NS5B pol V405I mutant	4ADP	1.90	$P2_12_12_1$		17% PEG 4000 0.05 M Tri-Na Citrate, pH 6.5	(Scrima *et al.*, 2012)
114	Hepatitis C virus – J4	RNA pol W550N mutant	4RY5	2.71	$P2_12_12_1$	Hanging drop (18°C)	50 mM MES, pH 5.0 20% PEG 4000 5% Glycerol	(Cherry *et al.*, 2015)
115	Hepatitis C virus – J4	RNA pol W550A mutant	4RY6	2.52	$P2_12_12_1$	Hanging drop (18°C)		
116	Hepatitis C virus	RNA pol	4RY7	3.00	$P2_12_12_1$	Hanging drop (18°C)		

	– J4	D559E mutant						
117	Hepatitis C virus	NS5B 2A JFH-1 with E86Q, E87Q, S15G, C223H, V321I and DELTA8 mutations (Apo)	4WT9	2.50	P6$_5$	Sitting drop (16°C)	30% PEG 550 MME 0.1 M HEPES, pH 7.5 50 mM MgCl$_2$	(Appleby et al., 2015)
118	Hepatitis C virus	NS5B 2A JFH-1 with S15G, E86Q, C233H, V321I and DELTA8 mutations with UDP, Mn^{2+}	4WTA	2.80	P6$_5$	Sitting drop (16°C)	25% PEG 550 MME 0.1 M HEPES, pH 7.5 50 mM MgCl$_2$	
119	Hepatitis C virus	NS5B 2A JFH-1 with S15G, E86Q, C233H, V321I and DELTA8 mutations with CDP, Mn^{2+}	4WTC	2.75	P6$_5$	Sitting drop (16°C)		
120	Hepatitis C virus	NS5B 2A	4WTD	2.70	P6$_5$	Sitting drop (16°C)		

		JFH-1 with S15G, E86Q, C233H, V321I and DELTA8 mutations with ADP, Mg^{2+}				
121	Hepatitis C virus	NS5B 2A JFH-1 with S15G, E86Q, C233H, V321I and DELTA8 mutations with GDP, Mg^{2+}	4WTE	2.90	P6$_5$	Sitting drop (16°C)
122	Hepatitis C virus	NS5B 2A JFH-1 with S15G, E86Q, C233H, V321I and DELTA8 mutations with GS-639475, Mg^{2+}	4WTF	2.65	P6$_5$	Sitting drop (16°C)
123	Hepatitis C virus	NS5B 2A JFH-1 with S15G, E86Q,	4WTG	2.90	P6$_5$	Sitting drop (16°C)

		C233H, V321I and DELTA8 mutations with GS-607596, Mg^{2+}				
124	Hepatitis C virus	NS5B 2A JFH-1 with S15G, E86Q, C233H, V321I mutations with RNA templates, Mg^{2+} GDP	4WTI	2.80	$P6_5$	Sitting drop (16°C)
125	Hepatitis C virus	NS5B 2A JFH-1 with S15G, E86Q, C233H, V321I mutations with RNA templates, Mg^{2+} ADP	4WTJ	2.20	$P6_5$	Sitting drop (16°C)
126	Hepatitis C virus	NS5B 2A JFH-1 with S15G, E86Q,	4WTK	2.50	$P6_5$	Sitting drop (16°C)

		C233H, V321I mutations with RNA templates, Mg^{2+} CDP						
127	Hepatitis C virus	NS5B 2A JFH-1 with S15G, E86Q, C233H, V321I mutations with RNA templates, Mg^{2+} UDP	4WTL	2.00	$P6_5$	Sitting drop (16°C)		
128	Hepatitis C virus	NS5B 2A JFH-1 with S15G, E86Q, C233H, V321I mutations with RNA templates, Mg^{2+} UDP	4WTM	2.15	$P6_5$	Sitting drop (16°C)		
129	Hepatitis C Virus	RNA pol apo-form	1NB4	2.00	$P2_12_12_1$	(18°C)	50 mM MES, pH 5.0 20% PEG 4000	(O'Farrell *et al.*, 2003)
130	Hepatitis C Virus	RNA pol with	1NB6	2.60	$P2_12_12_1$	(18°C)		

25

		UTP				10% Glycerol	
131	Hepatitis C Virus	RNA pol with short RNA template	1NB7	2.90	$P2_12_12_1$	(18°C)	5 mM DTT	
132	Human Norovirus	RdRp with inhibitor PPNDS	4LQ3	2.60	I222	Sitting drop (20°C)	1.2 M Na Citrate	(Tarantino *et al.*, 2014)
133	Human Norovirus	RdRp in complex with NAF2	4LQ9	2.04	I222	Sitting drop (20°C)	0.125 M NaCl	
							0.1 M Na cacodylate	
134	Human Norovirus	Pol bound to suramin derivative	4NRT	2.02	I222	Sitting drop (20°C)	1.2 M Na citrate,	(Croci, Pezzullo*, et al.*, 2014)
							0.125 M NaCl	
							0.1 M Na cacodylate, pH 6.2	
135	Human Rhinovirus 16	RdRp	1TP7	2.40	$P2_1$	Sitting drop (22°C)	40% PEG 4000	(Appleby *et al.*, 2005)
							0.1 M Na citrate pH 5.6,	
							35 mM $(NH_4)_2SO_4$	
							5% Glycerol	
							5 mM DTT	
136	Infectious bursal disease virus	RdRp VP1	2PGG	2.50	$P6_122$	Hanging drop (20°C)	0.1 M HEPES, pH 7.5	
							1.3 M Na malonate	(Pan *et al.*, 2007)

							10 mM NaI	
137	Infectious bursal disease virus	VP1 pol with oligopeptide	2QJ1	3.48	$P6_122$	Hanging drop (20°C)	10-12% PEG 3350 0.3-0.5 M LiNO$_3$, pH 6.5-8.0	(Garriga *et al.*, 2007)
138	Infectious bursal disease virus	RdRp	2PUS	2.40	$P6_122$	Hanging drop (25°C)		
139	Infectious bursal disease virus	VP1 pol with oligopeptide	2R70	2.70	$P6_122$	Hanging drop (20°C)	5% PEG 3350 0.4 M LiNO$_3$ 0.1 M Tris, pH 7.3	
140	Infectious bursal disease virus	VP1 pol with Mg^{2+} ion	2R72	3.15	$P6_122$	Hanging drop (20°C)	10% PEG 3350 0.4 M LiNO$_3$ 0.1 M MES, pH 6.0	
141	Infectious Pancreatic Necrosis Virus	VP1-VP3 complex	3ZED	2.20	$P2_12_12$		20% (w/v) PEG 3350 0.2 M KF, pH 7.5	(Bahar *et al.*, 2013)
142	Infectious Pancreatic Necrosis Virus	RNA polymerase VP1	2YI8	2.30	$P2_12_12_1$	Sitting drop	18-20% PEG 3350 0.09-0.1 M Bis-Tris Propane pH 7.5	(Graham *et al.*, 2011)
143	Infectious Pancreatic Necrosis Virus	RNA polymerase VP1	2YI9	2.20	$P2_12_12_1$	Sitting drop	0.18-0.2 M Na Citrate	
144	Infectious	RNA	2YIA	3.02	$P2_12_12_1$	Sitting drop		

	Pancreatic Necrosis Virus	polymerase VP1					
145	Infectious Pancreatic Necrosis Virus	RNA polymerase VP1	2YIB	3.80	$P2_12_12_1$	Sitting drop	20% PEG 3350 0.1 M Bis-Tris propane, pH 7.5 0.2 M Na Citrate 20 mM ATP 5% MPD 10 mM NaOH	
146	Influenza C virus	RdRp	5D9A	4.30	$P2_12_12_1$	Sitting drop (20°C)	0.2 M NaCl 25% PEG 4000 0.1 M HEPES, pH 7.5	(Hengrung *et al.*, 2015)
147	Influenza C virus	RdRp	5D98	3.90	$P4_32_12$	Sitting drop (20°C)	Morpheus condition G2: 10% PEG 8000, 20% ethylene glycol 0.02 M carboxylic acids 0.1 M MES/imidazole	
148	Japanese Encephalitis virus	RdRp	4MTP	3.65	$P2_12_12_1$	Hanging drop (25°C)	10-15% PEG 5000 MME 0.1 M Tris-HCl, pH 8.0 0.2 M NaSCN	(Surana *et al.*, 2014)

149	Murine Norovirus	RdRp	3NAH	2.75	C2	Hanging drop	1 M $(NH_4)_2SO_4$	To Be Published
150	Murine Norovirus	RdRp	3NAI	2.55	C2	Hanging drop (4°C)	0.1 M Cacodylate pH 6.5	
151	Norwalk Virus	Polymerase (Triclinic)	1SH0	2.17	P1	Hanging drop (22°C)	24% PEG 8000 0.1-0.2 M $(NH_4)_2SO_4$	(Ng *et al.*, 2004)
152	Norwalk Virus	Polymerase (Metal-free, Centered Orthorhombic)	1SH2	2.30	C222$_1$	Hanging drop (22°C)	50 mM Tris-HCl, pH 7.5 15 % Glycerol 14 mM 2-mercaptoethanol	
153	Norwalk Virus	Polymerase (MgSO4 crystal form)	1SH3	2.95	P2$_1$2$_1$2$_1$	Hanging drop (22°C)		
154	Murine Norovirus	RdRp	3MWV	2.20	P2$_1$2$_1$2$_1$	(11°C)	0.1 M MES, pH 5.4 21% PEG 5000 MME 0.4 M $(NH_4)_2SO_4$ 10% Glycerol	(LaPlante *et al.*, 2010)
155	Murine Norovirus	RdRp	3QID	2.50	C2	Hanging drop (22°C)	1.26 M $(NH_4)_2SO_4$ 0.1 M Cacodylate pH 6.5	(Lee *et al.*, 2011)
156	Murine Norovirus	RdRp with 2 thiouridine (2TU)	3SFG	2.20	C2	Hanging drop (4°C)	2 M $(NH_4)_2SO_4$ Cacodylate pH 6.5 0.2 M NaCl	(Alam *et al.*, 2012)

157	Murine Norovirus	RdRp with ribavirin	3SFU	2.50	C2	Hanging drop (20°C)	1.26 M (NH₄)₂SO₄ CHES, pH 9.5 0.2 M NaCl	
158	Murine Norovirus	Polymerase bound to NF023	3UPF	2.60	C2	Hanging drop (20°C)	1.5 M (NH₄)₂SO₄, 11% Glycerol 50 mM Tris pH 8.4	
159	Murine Norovirus	Polymerase with Suramin	3UR0	2.45	C2	Hanging drop (20°C)	1.3 M (NH₄)₂SO₄ 10% Glycerol 0.1 M Tris, pH 8.4	
160	Murine Norovirus	Polymerase with a suramin derivative	4NRU	2.30	P 2₁	Microbatch	1.6 M (NH₄)₂SO₄ 12% Glycerol 0.1 M Tris-HCl pH 8.4	(Croci, Pezzullo, *et al.*, 2014)
161	Murine Norovirus	RdRp in complex with PPNDS	4O4R	2.40	C2	Macrobatch (20°C)	1.6 M (NH₄)₂SO₄ 12% Glycerol 0.1 M Tris-HCl pH 8.4	(Croci, Tarantino, *et al.*, 2014)
162	Poliovirus	Polymerase full length apo	1RA6	2.00	P6₅	Hanging drop (16°C)	1.5 M Na Acetate, 0.1 M Cacodylic acid, pH 7.1	(Thompson & Peersen, 2004)
163	Poliovirus	Polymerase with GTP	1RA7	2.35	P6₅	Hanging drop (16°C)	2 mM DTT	

164	Poliovirus	Pol with 68 residues N-term truncation	1RAJ	2.50	P3$_1$2$_1$	Hanging drop (16°C)	1.5 M Ammonium Formate, 0.1 M NaCl, 0.05 M HEPES, pH 7.0, 2 mM DTT	
165	Poliovirus	3D polymerase	1RDR	2.40	P3$_1$2$_1$	Hanging drop (16°C)		
166	Poliovirus	Polymerase G1A mutant	1TQL	2.30	P6$_5$	Hanging drop (16°C)	2M Na-Acetate, 2 mM DTT 0.1 M Cacodylic acid, pH 7.1	
167	Poliovirus	RdRp 3Dpol G64S mutant	2IJF	3.00	P6$_5$	Hanging drop (20°C)	2 M NaOAc 0.1 M HEPES, pH 7.0	(Marcotte *et al.*, 2007)
168	Poliovirus	Polymerase with ATP and Mg^{2+}	2ILY	2.60	P6$_5$	Hanging drop (16°C)	2 M Na Acetate 0.1 M Cacodylic acid, pH 7.1 2 mM DTT	(Thompson *et al.*, 2007)
169	Poliovirus	Polymerase with GTP and Mn^{2+}	2ILZ	2.50	P6$_5$	Hanging drop (16°C)		
170	Poliovirus	Polymerase with CTP and Mn^{2+}	2IM0	2.25	P6$_5$	Hanging drop (16°C)		
171	Poliovirus	Polymerase with CTP and Mn^{2+}	2IM1	2.50	P6$_5$	Hanging drop (16°C)		

172	Poliovirus	Polymerase with UTP and Mn^{2+}	2IM2	2.35	$P6_5$	Hanging drop (16°C)		
173	Poliovirus	Polymerase with UTP and Mn^{2+}	2IM3	2.60	$P6_5$	Hanging drop (16°C)		
174	Poliovirus	Polymerase C290I loop mutant	4NLO	2.20	$P6_5$	Hanging drop (16°C)	0.25 M Na Acetate 0.1 M Cacodylic acid, pH 7.0 2 mM DTT, 30% PEG 400	(Sholders & Peersen, 2014)
175	Poliovirus	Polymerase C290V loop mutant	4NLP	2.20	$P6_5$	Hanging drop (16°C)		
176	Poliovirus	Polymerase C290F loop mutant	4NLQ	2.30	$P6_5$	Hanging drop (16°C)		
177	Poliovirus	Polymerase C290S loop mutant	4NLR	1.85	$P6_5$	Hanging drop (16°C)		
178	Poliovirus	Polymerase S288A loop mutant	4NLS	2.00	$P6_5$	Hanging drop (16°C)		
179	Poliovirus	Polymerase S291P loop	4NLT	2.50	$P6_5$	Hanging drop (16°C)		

		mutant						
180	Poliovirus	Polymerase G289A loop mutant	4NLU	1.96	P6$_5$	Hanging drop (16°C)		
181	Poliovirus	Polymerase G289A/C290F loop mutant	4NLV	2.30	P6$_5$	Hanging drop (16°C)		
182	Poliovirus	Polymerase G289A/C290I loop mutant	4NLW	2.10	P6$_5$	Hanging drop (16°C)		
183	Poliovirus	Polymerase G289A/C290 V loop mutant	4NLX	2.60	P6$_5$	Hanging drop (16°C)		
184	Poliovirus	Polymerase C290E loop mutant	4NLY	2.30	P6$_5$	Hanging drop (16°C)		
185	Poliovirus	RdRp low-fidelity mutant 3D pol H273R	4R0E	3.00	P6$_5$	(20°C)	2 M Na Acetate 0.1 M Na Cacodylate, pH 6.8	(Moustafa *et al.*, 2014)
186	Pseudomonas phage Phi6	RdRp	1HHS	2.00	P2$_1$		10% PEG 8000 0.1 M MES 2 mM MnCl$_2$	(Butcher *et al.*, 2001)

187	Pseudomonas phage Phi6	RdRp	2JLF	3.20	P32		15-20% PEG 4000 8.5% Isopropanol 15% Glycerol 0.1 M HEPES, pH 7.5	(Poranen *et al.*, 2008)
188	Pseudomonas phage Phi6	RdRp	4A8F	3.30	P2$_1$		20% PEG 4000 0.1 M HEPES, pH 7.5	(Wright *et al.*, 2012)
189	Pseudomonas phage Phi6	RdRp	4A8K	2.90	P2$_1$		8.5% Isopropanol 15% Glycerol	
190	Pseudomonas phage Phi6	RdRp	4A8M	2.90	P2$_1$		2 mM MnCl$_2$	
191	Pseudomonas phage Phi6	RdRp	4A8O	2.67	P2$_1$			
192	Pseudomonas phage Phi6	RdRp	4A8Q	3.00	P2$_1$		20% PEG 2000 0.1 M MES, pH 6.5	
193	Pseudomonas phage Phi6	RdRp	4A8S	2.90	P2$_1$			
194	Pseudomonas phage Phi6	RdRp	4A8Y	3.40	P2$_1$			
195	Rabbit Hemorrhagic	RdRp with Lu^{3+}	1KHV	2.50	P2$_1$2$_1$2$_1$	Hanging drop (25°C)	10–12% PEG 8000 0.1 M Tris-HCl, pH 7.5	(Ng *et al.*, 2002)

	Disease Virus						0.2 M Na thiocyanate
							0.1 M L-proline
							15% Glycerol
							7% 1,6-hexanediol,
							0.1% CHAPS,
							5 mM $CaCl_2$
							2 mM $MgCl_2$
196	Rabbit Hemorrhagic Disease Virus	RdRp with Mn^{2+}	1KHW	2.70	$P2_12_12_1$	Hanging drop (25°C)	10-12% PEG 8000
							0.1 M Tris, pH 7.5
							0.2 M sodium thiocyanate
							0.1 M L-proline
							15% (w/v) glycerol
							7% (v/v) 1,6-hexanediol
							0.1% (w/v) CHAPS
							5 mM $CaCl_2$,
							2 mM $MgCl_2$
197	Thielavia terres	RdRp QDE-1	5FSW	3.19	$P2_1$		0.1 M Tris, pH 8.0 (Qian *et al.*, 2016)
							75 mM NaCl
							10% PEG 10000

198	Thosea asigna virus	RdRp complexed with CDP	5CX6	2.10	P2$_1$2$_1$2$_1$	Sitting drop (20°C)	12% PEG 8000 0.75 M Li$_2$SO$_4$	(Ferrero *et al.*, 2015)
199	Thosea asigna virus	RdRp with ATP and ssRNA	5CYR	3.50	I222	Sitting drop (20°C)		
200	Thosea asigna virus	RdRp complexed with Lu^{3+}	4XHA	3.00	C222$_1$	Sitting drop (20°C)		
201	Thosea asigna virus	RdRp native	4XHI	2.15	P2$_1$2$_1$2	Sitting drop (20°C)		

Table S2   The calculated volume for each stock solution used in the distinct conditions of the screen is provided (Total volume: 10 ml).

	1	2	3	4	5	6	7	8	9	10	11	12
A	0.5 ml MES, pH 5.0 7.3 ml NaCl 1.5 ml Glycerol 0.7 ml H₂O	0.5 ml MMT, pH 5.5 7.3 ml NaCl 1.5 ml Glycerol 0.7 ml H₂O	0.5 ml (CH₃)₂AsO₂Na, pH 6.5 7.3 ml NaCl 1.5 ml Glycerol 0.7 ml H₂O	0.85 ml HEPES, pH 7.0 7.3 ml NaCl 1.5 ml Glycerol 0.35 ml H₂O	0.85 ml Tris, pH 7.5 3.18 ml (NH₄)₂SO₄ 2.5 ml Glycerol 3.46 ml H₂O	0.5 ml Tris, pH 7.5 3.22 ml (NH₄)₂SO₄ 2.45 ml Glycerol 3.83 ml H₂O	0.5 ml Tris, pH 8.0 3.22 ml (NH₄)₂SO₄ 2.45 ml Glycerol 3.83 ml H₂O	0.5 ml Tris, pH 8.5 3.22 ml (NH₄)₂SO₄ 2.45 ml Glycerol 3.83 ml H₂O	0.5 ml SPG, pH 9.0 3.22 ml (NH₄)₂SO₄ 2.45 ml Glycerol 3.83 ml H₂O	1 ml MES, pH 5.0 0.02 ml MnCl₂ 0.02 ml MgCl₂ 3.25 ml (NH₄)₂SO₄ 5.71 ml H₂O	1 ml Bis-Tris, pH 6.1 0.01 ml DTT 0.2 ml NiSO₄ 30.25 ml (NH₄)₂SO₄ 5.54 ml H₂O	1 ml (CH₃)₂AsO₂Na, pH 6.5 2.45 ml (NH₄)₂SO₄ 6.5 ml H₂O
B	1 ml (CH₃)₂AsO₂Na, pH 6.5 0.4 ml NaCl 5 ml (NH₄)₂SO₄ 3.6 ml H₂O	0.5 ml HEPES, pH 7.0 0.2 ml NaCl 3.75 ml (NH₄)₂SO₄ 0.02 ml DTT 5.53 ml H₂O	0.5 ml HEPES, pH 7.5 0.2 ml NaCl 3.75 ml (NH₄)₂SO₄ 0.02 ml DTT 5.53 ml H₂O	0.5 ml Tris, pH 8.0 3.75 ml (NH₄)₂SO₄ 10.1 ml Glycerol 4.65 ml H₂O	0.5 ml Tris, pH 8.5 3.75 ml (NH₄)₂SO₄ 10.1 ml Glycerol 4.65 ml H₂O	2 ml CHES, pH 9.5 0.4 ml NaCl 30.15 ml (NH₄)₂SO₄ 4.45 ml H₂O	2 ml CAPS, pH 10.0 1 ml Li₂SO4 5ml (NH₄)₂SO₄ 2 ml H₂O	1 ml MMT, pH 5.0 5.333 ml K/Na Tartrate 3.667 ml H₂O	1 ml MMT, pH 5.5 5.333 ml K/Na Tartrate 0.05 ml of PEG 550 MME 3.617 ml H₂O	1 ml MMT, pH 6 5.333 ml K/Na Tartrate 3.667 ml H₂O	1 ml (CH₃)₂AsO₂Na, pH 6.5 5.333 ml K/Na Tartrate 3.667 ml H₂O	1 ml HEPES, pH 7.0 5.333 ml K/Na Tartrate 0.1 ml of PEG 400 3.567 ml H₂O
C	1 ml HEPES, pH 7.5 5.333 ml K/Na Tartrate 3.667 ml H₂O	1 ml Tris-HCl, pH 8.5 5.333 ml K/Na Tartrate 0.1 ml PEG 5000 MME 3.567 ml H₂O	1 ml Tris-HCl, pH 8.5 5.333 ml K/Na Tartrate 0.2 ml PEG 2000 MME 3.467 ml H₂O	1 ml (CH₃)₂AsO₂Na, pH 6.5 0.25 ml NaCl 4 ml Na₃C₆H₅O₇ 4.75 ml H₂O	1 ml HEPES, pH 7.5 0.1 ml NaI 3.823 ml C₃H₂O₄Na₂ 5.077 ml H₂O	1 ml HEPES, pH 7.0 6.67 ml C₂H₃NaO₂ 0.1 ml PEG 550 MME 20.233 ml H₂O	1 ml (CH₃)₂AsO₂Na, pH 7.1 6.67 ml C₂H₃NaO₂ 2.33 ml H₂O	0.5 ml MES, pH 5.0 2 ml NaCl 2 ml PEG 400 0.05 ml DTT 5.45 ml H₂O	1 ml Bis-Tris propane, pH 6.5 00.125 ml (NH₄)₂SO₄ 3 ml PEG 550 MME 5.875 ml H₂O	1 ml HEPES, pH 7.5 0.5 ml MgCl₂ 3 ml PEG 550 MME 5.5 ml H₂O	1 ml HEPES, pH 7.5 0.5 ml MnCl₂ 3 ml PEG 550 MME 5.5 ml H₂O	0.5 ml Tris, pH 7.5 0.2 ml NH₄OAc 2.5 ml PEG 550 MME 6.8 ml H₂O
D	1 ml Tris, pH 8.0 2.5 ml PEG 550 MME 6.5 ml H₂O	1 ml Tris, pH 8.0 2 ml PEG 550 MME 7 ml H₂O	1 ml Tris, pH 8.5 2 ml PEG 550 MME 7 ml H₂O	1 ml Bicine, pH 9.0 2.5 ml PEG 550 MME 6.5 ml H₂O	0.5 ml MES, pH 6.5 0.5 ml (NH₄)₂SO₄ 0.25 ml NH₄OAc 2.5 ml PEG 1000 60.25 ml dH₂O	1 ml MES, pH 8.0 2.5 ml PEG 1500 6.5 ml H₂O	1 ml MES, pH 6.5 5 ml PEG 2000 4 ml H₂O	00.1 ml NH₄OAc, pH 5.0 0.5 ml (NH₄)₂SO₄ 6 ml PEG 2000 MME 3.4 ml H₂O	1 ml HEPES, pH 7.0 8.333 ml C₄H₄O₄ 00.1 ml PEG 2000 MME 0.567 ml H₂O	1 ml Na₃C₆H₅O₇, pH 5.5 3.6 ml PEG 3350 1.4 ml Glycerol 4 ml H₂O	1 ml Bis-Tris propane, pH 6.0 0.5 ml NH₄OAc 6 ml PEG 3350 2.5 ml H₂O	1 ml MES, pH 6.0 4 ml LiNO₃ 2 ml PEG 3350 3 ml H₂O
E	1 ml Bis-Tris Propane, pH 7.5 2 ml Na₃C₆H₅O₇ 4 ml PEG 3350 3 ml H₂O	1 ml Bis-Tris Propane, pH 7.5 1 ml Na₃C₆H₅O₇ 4 ml PEG 3350 0.5 ml MPD 0.05 ml MnCl₂ 0.033 ml ATP 0.02 ml NaOH 3.397 ml H₂O	1 ml MMT Buffer pH 8.0 3.5 ml LiNO₃ 2.4 ml PEG 3350 30.1 ml H₂O	0.333 ml C₂H₃NaO₂, pH 4.7 0.125 ml (NH₄)₂SO₄ 4 ml PEG 4000 0.05 ml DTT 5.492 ml H₂O	0.5 ml Na₃C₆H₅O₇, pH 4.9 50.2 ml PEG 4000 0.75 ml Glycerol 3.550 ml H₂O	0.5 ml MES, pH 5.0 0.05 ml DTT 4 ml PEG 4000 1 ml Glycerol 4.45 ml H₂O	0.5 ml MES, pH 5.0 4 ml PEG 4000, 0.5 ml Glycerol 5 ml H₂O	1 ml Na₃C₆H₅O₇, pH 5.0 4 ml PEG 4000 0.05 ml DTT 1 ml Glycerol 3.950 ml H₂O	0.333 ml C₂H₃NaO₂, pH 5.0 0.6 ml NaCl 3.6 ml PEG 4000 0.004 ml β-mercaptoethanol 5.463 ml H₂O	0.333 ml C₂H₃NaO₂, pH 5.0 0.6 ml NaCl 30.2 ml PEG 4000 1 ml Glycerol 0.004 ml β-mercaptoethanol 4.863 ml H₂O	0.5 ml Na₃C₆H₅O₇, pH 5.6 0.2 ml NH₄OAc 6.6 ml PEG 4000 0.4 ml γ-butyrolactone 2.3 ml H₂O	1 ml Na₃C₆H₅O₇, pH 5.6 0.087 ml (NH₄)₂SO₄ 8 ml PEG 4000 0.5 ml Glycerol 0.05 ml DTT 0.363 ml H₂O
F	1 ml MES, pH 6.0 2 ml Mg(CH3COO)₂ 6 ml PEG 4000 0.4 ml γ- butyrolactone 0.6 ml H₂O	0.333 ml C₂H₃NaO₂, pH 6.0 0.6 ml NaCl 2.8 ml PEG 4000 0.004 ml β-mercaptoehanol 60.263 ml dH₂O	0.5 ml Na₃C₆H₅O₇, pH 6.5 3.4 ml PEG 4000 60.1 ml H₂O	0.333 ml C₂H₃NaO₂, pH 6.5 0.350 ml NH₄OAc 5 ml PEG 4000 4.317 ml H₂O	1 ml (CH₃)₂AsO₂Na, pH 6.5 2 ml Mg(CH₃COO)₂ 6 ml PEG 4000 1 ml H₂O	0.5 ml Na₃C₆H₅O₇, pH 6.8 0.8 ml PEG 4000 0.7 ml Isopropanol 8 ml H₂O	0.5 ml Tris, pH 7.5 50.2 ml PEG 4000 0.75 ml Glycerol 3.55 ml H₂O	1 ml Na-HEPES, pH 7.5 00.1 ml CaCl₂ 0.4 ml NaCl 5 ml PEG 4000 1 ml Glycerol 2.5 ml H₂O	1 ml HEPES, pH 7.5 4 ml PEG 4000 0.85 ml Isopropanol 1.5 ml Glycerol 2.65 ml H₂O	1 ml HEPES, pH 7.5 0.02 ml MnCl₂ 4 ml PEG 4000 0.85 ml Isopropanol 1.5 ml Glycerol 2.63 ml H₂O	1 ml Tris, pH 8.0 0.02 ml MnCl₂ 4 ml PEG 4000 0.85 ml Isopropanol 1.5 ml Glycerol 2.63 ml H₂O	1 ml Tris, pH 8.0 0.02 ml MnCl₂ 4 ml PEG 4000 0.85 ml Isopropanol 1.5 ml Glycerol 2.63 ml H₂O
G	1 ml Bicine, pH 9.0 0.02 ml MnCl₂ 4 ml PEG 4000 0.85 ml Isopropanol 1.5 ml Glycerol 2.63 ml dH₂O	3.75 ml Li₂SO₄ 2.4 ml PEG 8000 3.85 ml H₂O	0.333 ml C₂H₃NaO₂, pH 5.0 0.5 ml (NH₄)₂SO₄ 5.4 ml PEG 5000 MME 3.767 ml H₂O	1 ml MES, pH 5 1 ml (NH₄)₂SO₄ 40.2 ml PEG 5000 MME 1 ml Glycerol 2.8 ml dH₂O	0.5 ml Na₃C₆H₅O₇, pH 5.5 1.6 ml PEG 8000 0.5 ml Isopropanol 7.4 ml H₂O	1 ml MES, pH 6.0 00.1 ml MnCl₂ 2.8 ml PEG 8000 1.4 ml Isopropanol 0.05 ml TCEP 4.65 ml H₂O	1 ml (CH₃)₂AsO₂Na, pH 6.4 2 ml Mg(CH3COO)₂ 3 ml PEG 8000 4 ml H₂O	1 ml MES, pH 6.5 0.5 ml (NH₄)₂SO₄ 5 ml PEG 5000 MME 3.5 ml H₂O	1 ml M Na₃C₆H₅O₇, pH 6.5 1 ml PEG 8000, 0.5 ml Isopropanol 7.5 ml H₂O	1 ml Buffer System 1, pH 6.5 (Morpheus) 0.2 ml C₄H₆O₅ 2 ml PEG 8000 2 ml Ethylene Glycol 4.8 ml H₂O	1 ml MES, pH 6.5 0.02 ml M MnCl₂ 2 ml PEG 8000 6.98 ml H₂O	1 ml HEPES pH 7.5 2 ml PEG 8000 0.8 ml Ethylene Glycol 60.2 ml H₂O
H	1 ml Tris, pH 7.5 0.01 ml Tween-20 0.05 ml CaCl₂ 0.02 ml MgCl₂ 2.4 ml PEG 8000 1.5 ml Glycerol 1.4 ml 1,6-hexanediol	0.5 ml Tris, pH 7.5 0.5 ml (NH₄)₂SO₄ 4.8 ml PEG 8000 1.5 ml Glycerol 2.7 mldH₂O	0.5 ml Tris, pH 7.5 0.25 ml (NH₄)₂SO₄ 0.2 ml MgSO₄ 4.8 ml PEG 8000 1.5 ml Glycerol 2.75 ml H₂O	0.5 ml Tris, pH 8.0 0.5 ml (NH₄)₂SO₄ 4.8 ml PEG 8000 1.5 ml Glycerol 2.7 ml H₂O	0.5 ml Tris, pH 8.5 0.5 ml (NH₄)₂SO₄ 4.8 ml PEG 8000 1.5 ml Glycerol 2.7 ml H₂O	1 ml Tris, pH 7.5 0.15 ml NaCl 2 ml PEG 10000 6.85 ml H₂O	1 ml Tris, pH 8.0 0.15 ml NaCl 2 ml PEG 10000 6.85 ml H₂O	1 ml Tris, pH 8.5 0.15 ml NaCl 2 ml PEG 10000 6.85 ml H₂O	2 ml NaH₂PO₄, pH 7.0 1.4 ml PEG 20000 6.6 ml H₂O	2 ml HEPES, pH 7.5 1.4 ml PEG 20000 6.6 ml H₂O	2 ml Tris, pH 8.0 1.4 ml PEG 20000 6.6 ml H₂O	2 ml HEPES, pH 8.5 1.4 ml PEG 20000 6.6 ml H₂O

Table S3 List of chemicals used in the preparation of the crystallization screen. The table provides the names, source of the chemicals and their catalogue numbers and stock solutions.

Reagent	Company	Catalogue No.	Stock solution
1,6-Hexanediol	Sigma	240117	50% (v/v)
Ammonium Acetate	Acros Organics /Fisher	AC401152500	1 M
Ammonium Sulfate	Sigma	A4418	4 M
ATP	Acros Organics /Fisher	AC102800100	6 M
Bicine	Bio Basic Inc.	BB0266	1 M
Bis-Tris Propane	Melford	B7510	1 M
Buffer System 1 - Morpheus	Molecular Dimension	MD2-100-100	100% (v/v)
γ-Butyrolactone	Aldrich	B103608	100% (w/v)
Calcium Chloride	Sigma-Aldrich	C3306	1 M
CHAPS	Melford	B2006	0.5 M
CHES	Bio Basic Inc.	CB0115	0.5 M
DTT	Fluka	43817	1 M
Ethylene Glycol	Alfa Aesar	A11591	100% (w/v)
Glycerol	Melford	G1345	100% (w/v)
HEPES	Melford	B2001	1 M
Isopropanol	Fisher Scientific	BP2618	100% (v/v)
Lithium Nitrate	Sigma-Aldrich	227986	1 M
Lithium Sulfate	Acros Organics /Fisher	218331000	2 M
L-Proline	Melford	P0717	100 mM
Magnesium Acetate	Sigma-Aldrich	2286448	1 M
Magnesium Chloride	Melford	M0533	1 M
Malic Acid	Acros Organics /Fisher	125252500	1 M
Manganese Chloride	Alfa Aesar	11868	1 M
MES	Sigma-Aldrich	M2933	1 M
MPD	Sigma-Aldrich	112100	100% (w/v)
Nickel Sulfate	Fisher Scientific	10568810	1 M

PEG 400	Sigma-Aldrich	202398	100% (w/v)
PEG 1000	Acros Organics /Fisher	AC192250010	50% (w/v)
PEG 1500	Fluka	81210	50% (w/v)
PEG 2000	VWR	200007-386	50% (w/v)
PEG 3350	Sigma-Aldrich	202444	50% (w/v)
PEG 4000	Sigma-Aldrich	95904	50% (w/v)
PEG 8000	Sigma-Aldrich	89510	50% (w/v)
PEG 10000	Sigma-Aldrich	81280	50% (w/v)
PEG 20000	Sigma-Aldrich	95172	30% (w/v)
PEG 550 MME	Aldrich	202487	100% (w/v)
PEG 2000 MME	VWR	AAA17925-30	30% (w/v)
PEG 5000 MME	Sigma-Aldrich	81323	50% (w/v)
Sodium Acetate	Sigma-Aldrich	52889	3 M
Sodium Cacodylate	Sigma-Aldrich	C4945	1 M
Sodium Chloride	Sigma-Aldrich	S3014	5 M
Sodium Citrate	Alfa Aesar	L12557	1 M
Sodium Dihydrogen Phosphate	Melford	S2318	1 M
Sodium Hydroxide	Sigma-Aldrich	221465	5 M
Sodium Iodide	Millipore Merck	106523	2 M
Sodium Malonate	Sigma-Aldrich	63409	3.4 M
Sodium Potassium Tartrate	Sigma-Aldrich	217255	2 M
Succinic Acid	Acros Organics /Fisher	AC158742500	2 M
TCEP	Melford	T2650	1 M
Tris	Melford	B2005	1 M
Tri-Sodium Citrate	Acros Organics /Fisher	227130010	1 M
Tween-20	Millipore Merck	655204	100% (w/v)
β-Mercaptoethanol	Acros Organics /Fisher	125472500	14.3 M

Table S4   Summary of approximate diffraction limits obtained for Dengue RdRp3 crystals in various well conditions of the crystallization screen.

Well Number	Resolution	Well Number	Resolution
A3	No diffraction	D6	10.0
A4	No diffraction	D7	3.0
A6	10.0	D11	12.0
A11	10.0	E1	7.0
A12	8.0	E2	4.5
B4	3.0	E4	2.9
B5	15.0	E6	20.0
B6	No diffraction	E8	4.0
B9	2.3	E12	5.0
B11	15.0	F1	15.0
B12	3.1	F2	12.0
C2	2.3	F3	17.0
C3	2.7	F9	14.0
C6	2.2	G1	2.3
D1	2.1	G2	2.3
D2	2.0	G4	6.0
D3	15.0	G8	8.0
D5	2.7	H4	No diffraction

Table S5   Data collection and structure refinement statistics of dengue RdRp3 structures obtained from different crystallization conditions in the RdRp Screen.

Well Number	B4	B9	B12	C2	C3	C6	D1	D2	D5	D7	E6	G1	G2
Unit-cell parameters	120.6, 57.8, 120.8, 90, 96.4, 90	162.9, 180.8, 58.1, 90, 90, 90	162.1, 180.0, 57.9, 90, 90, 90	160.8, 177.9, 57.9, 90, 90, 90	162.5, 179.6, 58.1, 90, 90, 90	161.4, 178.3, 58.0, 90, 90, 90	162.4, 180.0, 58.3, 90, 90, 90	161.5, 179.0, 58.0, 90, 90, 90	163.5, 180.6, 58.3, 90, 90, 90	163.8, 181.0, 58.3, 90, 90, 90	162.7, 179.7, 58.1, 90, 90, 90	162.8, 179.4, 58.1, 90, 90, 90	162.1, 179.5, 58.1, 90, 90, 90
Space group	$P2_1$	$C222_1$	$C222_1$	$C222_1$	$C222_1$	$C222_1$	$C222_1$	$C222_1$	$C222_1$	$C222_1$	$C222_1$	$C222_1$	$C222_1$
Resolution range	48.6 – 3.0	60.5 – 2.3	48.7 – 3.0	80.4 – 2.3	48.8 – 2.7	48.6 – 2.2	60.3 – 2.1	48.7 – 2.0	49.0 – 2.7	81.9 – 3.0	60.3 – 2.9	48.8 – 2.3	81.1 – 2.3
Total reflections	100931 (14551)	146729 (22230)	72867 (9527)	166100 (25269)	86350 (13120)	242356 (33763)	167787 (23649)	248250 (37775)	148497 (21746)	58720 (7835)	76136 (9760)	168413 (25106)	690005 (7092)
Unique reflections	33463 (4841)	38149 (5508)	15767 (2268)	37243 (5371)	23467 (3404)	42774 (6205)	49636 (7190)	55928 (8180)	25451 (3633)	17272 (2491)	19297 (2775)	37242 (5486)	36741 (3712)
Completeness (%)	99.4 (99.7)	98.9 (99.1)	99.6 (99.6)	99.7 (99.9)	98.8 (99.7)	99.5 (99.7)	99.0 (99.6)	98.1 (99.6)	99.5 (99.6)	97.3 (98.0)	99.7 (99.7)	99.2 (97.6)	96.2 (98.6)
Multiplicity	3.0 (3.0)	3.8 (4.0)	4.6 (4.2)	4.5 (4.7)	3.7 (3.8)	5.7 (5.4)	3.4 (3.3)	4.4 (4.6)	5.8 (6.0)	3.4 (3.1)	3.9 (3.5)	4.5 (4.6)	11.0 (3.0)
R merge (%)	13.9 (44.0)	8.6 (50.4)	15.5 (58.8)	10.0 (38.8)	13.6 (50.4)	7.7 (70.2)	8.4 (42.0)	9.8 (72.0)	10.2 (60.3)	14.4 (58.5)	10.8 (15.8)	6.6 (50.1)	4.7 (26.9)
I/∑I	6.8 (2.4)	10.9 (3.2)	8.2 (2.0)	9.3 (3.1)	10.6 (4.3)	15.1 (2.4)	8.5 (2.4)	9.8 (2.0)	14.4 (3.3)	6.4 (1.9)	9.4 (5.2)	13.9 (2.8)	14.5 (4.5)
R work/R free (%)	17.5/25.2	18.4/24.4	18.3/26.1	20.8/26.2	17.4/24.3	20.0/23.4	20.2/26.4	24.6/27.0	17.7/22.9	18.6/26.5	21.6/28.4	17.7/22.5	17.6/22.4
Wilson B (^{2})	54.1	33.0	58.4	28.1	27.8	28.7	25.9	24.3	28.6	52.6	33.2	41.0	33.3
r.m.s.d. bond length	0.018	0.013	0.016	0.013	0.013	0.012	0.012	0.013	0.013	0.017	0.014	0.012	0.012
r.m.s.d. bond angles	1.706	1.213	1.704	1.298	1.295	1.140	1.152	1.331	1.215	1.742	1.588	1.177	1.240
Ramachandran													
Favoured	90.0	96.0	97.0	95.3	94.7	96.2	96.7	96.7	96.7	88.1	96.6	95.7	96.3
Allowed	8.4	3.2	1.8	4.6	4.6	33	2.9	2.5	2.6	10.2	2.50	4.1	3.3
Outliers	1.6	0.9	1.2	0.2	0.7	0.5	0.4	1.3	0.7	1.8	0.9	0.2	0.4

Table S6   Details of missing regions in the structures, PEG and water molecules in the structure of dengue RdRp3 solved from the screen. Interestingly, the flexible regions in motif G (~ 454 – 469) and motif F (~ 406 – 419) are missing in all the structures consistently proving all the structures are in the closed confirmation.

Well Number on plate	B4	B9	B12	C2	C3	C6	D1	D2	D5	D7	E4	G1	G2
Resolution (Å)	3.0	2.3	3.0	2.3	2.7	2.2	2.1	2.0	2.7	3.0	2.9	2.3	2.3
Missing regions	Chain A 311 – 317 344 – 354 406 – 418 451 – 469 583 – 586 Chain B 310 – 317 344 – 356 406 – 418 453 – 469 583 –588	311 – 317 406 – 417 454 – 469	312 – 315 406 – 419 454 – 469	310 – 318 343 – 353 407 – 419 454 – 469 581 – 588	311 – 317 343 – 353 407 – 419 454 – 469 581 – 588	311 – 317 344 – 349 406 – 419 454 – 469 581 – 586	311 – 318 343 – 353 406 – 419 454 – 473 581 – 588	311 – 318 344 – 348 407 – 419 454 – 469 583 – 585	406 – 419 454 – 469	311 – 317 406 – 418 454 – 469	311 – 317 406 – 418 455 – 469	314 – 316 406 – 416 456 – 469	312 – 318 405 – 418 454 – 469
No. of PEG molecules	none	3	6	5	5	3	2	2	3 (1 –P6G)	5	4	5	6
No. of water molecules	35	348	90	222	223	334	871	367	256	92	213	254	272

References

Ago, H., Adachi, T., Yoshida, A., Yamamoto, M., Habuka, N., Yatsunami, K. & Miyano, M. (1999). *Structure* **7**, 1417-1426.

Alam, I., Lee, J. H., Cho, K. J., Han, K. R., Yang, J. M., Chung, M. S. & Kim, K. H. (2012). *Virology* **426**, 143-151.

Ando, I., Adachi, T., Ogura, N., Toyonaga, Y., Sugimoto, K., Abe, H., Kamada, M. & Noguchi, T. (2012). *Antimicrob Agents Chemother* **56**, 4250-4256.

Antonysamy, S. S., Aubol, B., Blaney, J., Browner, M. F., Giannetti, A. M., Harris, S. F., Hebert, N., Hendle, J., Hopkins, S., Jefferson, E., Kissinger, C., Leveque, V., Marciano, D., McGee, E., Najera, I., Nolan, B., Tomimoto, M., Torres, E. & Wright, T. (2008). *Bioorg Med Chem Lett* **18**, 2990-2995.

Appleby, T. C., Luecke, H., Shim, J. H., Wu, J. Z., Cheney, I. W., Zhong, W., Vogeley, L., Hong, Z. & Yao, N. (2005). *J Virol* **79**, 277-288.

Appleby, T. C., Perry, J. K., Murakami, E., Barauskas, O., Feng, J., Cho, A., Fox, D., 3rd, Wetmore, D. R., McGrath, M. E., Ray, A. S., Sofia, M. J., Swaminathan, S. & Edwards, T. E. (2015). *Science* **347**, 771-775.

Bahar, M. W., Sarin, L. P., Graham, S. C., Pang, J., Bamford, D. H., Stuart, D. I. & Grimes, J. M. (2013). *J Virol* **87**, 3229-3236.

Bressanelli, S., Tomei, L., Rey, F. A. & De Francesco, R. (2002). *J Virol* **76**, 3482-3492.

Butcher, S. J., Grimes, J. M., Makeyev, E. V., Bamford, D. H. & Stuart, D. I. (2001). *Nature* **410**, 235-240.

Campagnola, G., McDonald, S., Beaucourt, S., Vignuzzi, M. & Peersen, O. B. (2015). *J Virol* **89**, 275-286.

Canales, E., Carlson, J. S., Appleby, T., Fenaux, M., Lee, J., Tian, Y., Tirunagari, N., Wong, M. & Watkins, W. J. (2012). *Bioorg Med Chem Lett* **22**, 4288-4292.

Cherry, A. L., Dennis, C. A., Baron, A., Eisele, L. E., Thommes, P. A. & Jaeger, J. (2015). *J Virol* **89**, 2052-2063.

Choi, K. H., Gallei, A., Becher, P. & Rossmann, M. G. (2006). *Structure* **14**, 1107-1113.

Croci, R., Pezzullo, M., Tarantino, D., Milani, M., Tsay, S. C., Sureshbabu, R., Tsai, Y. J., Mastrangelo, E., Rohayem, J., Bolognesi, M. & Hwu, J. R. (2014). *PLoS One* **9**, e91765.

Croci, R., Tarantino, D., Milani, M., Pezzullo, M., Rohayem, J., Bolognesi, M. & Mastrangelo, E. (2014). *FEBS Lett* **588**, 1720-1725.

de Vicente, J., Hendricks, R. T., Smith, D. B., Fell, J. B., Fischer, J., Spencer, S. R., Stengel, P. J., Mohr, P., Robinson, J. E., Blake, J. F., Hilgenkamp, R. K., Yee, C., Adjabeng, G., Elworthy, T. R., Li, J., Wang, B., Bamberg, J. T., Harris, S. F., Wong, A., Leveque, V. J., Najera, I., Le Pogam, S., Rajyaguru, S., Ao-Ieong, G., Alexandrova, L., Larrabee, S., Brandl, M., Briggs, A., Sukhtankar, S. & Farrell, R. (2009). *Bioorg Med Chem Lett* **19**, 5652-5656.

de Vicente, J., Hendricks, R. T., Smith, D. B., Fell, J. B., Fischer, J., Spencer, S. R., Stengel, P. J., Mohr, P., Robinson, J. E., Blake, J. F., Hilgenkamp, R. K., Yee, C., Adjabeng, G., Elworthy, T. R., Tracy, J., Chin, E., Li, J., Wang, B., Bamberg, J. T., Stephenson, R., Oshiro, C., Harris, S. F., Ghate, M., Leveque, V., Najera, I., Le Pogam, S., Rajyaguru, S., Ao-Ieong, G., Alexandrova, L., Larrabee, S., Brandl, M., Briggs, A., Sukhtankar, S., Farrell, R. & Xu, B. (2009). *Bioorg Med Chem Lett* **19**, 3642-3646.

de Vicente, J., Hendricks, R. T., Smith, D. B., Fell, J. B., Fischer, J., Spencer, S. R., Stengel, P. J., Mohr, P., Robinson, J. E., Blake, J. F., Hilgenkamp, R. K., Yee, C., Zhao, J., Elworthy, T. R., Tracy, J., Chin, E., Li, J., Lui, A., Wang, B., Oshiro, C., Harris, S. F., Ghate, M., Leveque, V. J., Najera, I., Le Pogam, S., Rajyaguru, S., Ao-Ieong, G., Alexandrova, L., Fitch, B., Brandl, M., Masjedizadeh, M., Wu, S. Y., de Keczer, S. & Voronin, T. (2009). *Bioorg Med Chem Lett* **19**, 5648-5651.

Di Marco, S., Volpari, C., Tomei, L., Altamura, S., Harper, S., Narjes, F., Koch, U., Rowley, M., De Francesco, R., Migliaccio, G. & Carfi, A. (2005). *J Biol Chem* **280**, 29765-29770.

Dragovich, P. S., Blazel, J. K., Ellis, D. A., Han, Q., Kamran, R., Kissinger, C. R., LeBrun, L. A., Li, L. S., Murphy, D. E., Noble, M., Patel, R. A., Ruebsam, F., Sergeeva, M. V., Shah, A. M.,

Showalter, R. E., Tran, C. V., Tsan, M., Webber, S. E., Kirkovsky, L. & Zhou, Y. (2008). *Bioorg Med Chem Lett* **18**, 5635-5639.

Ellis, D. A., Blazel, J. K., Tran, C. V., Ruebsam, F., Murphy, D. E., Li, L. S., Zhao, J., Zhou, Y., McGuire, H. M., Xiang, A. X., Webber, S. E., Zhao, Q., Han, Q., Kissinger, C. R., Lardy, M., Gobbi, A., Showalter, R. E., Shah, A. M., Tsan, M., Patel, R. A., LeBrun, L. A., Kamran, R., Bartkowski, D. M., Nolan, T. G., Norris, D. A., Sergeeva, M. V. & Kirkovsky, L. (2009). *Bioorg Med Chem Lett* **19**, 6047-6052.

Ellis, D. A., Blazel, J. K., Webber, S. E., Tran, C. V., Dragovich, P. S., Sun, Z., Ruebsam, F., McGuire, H. M., Xiang, A. X., Zhao, J., Li, L. S., Zhou, Y., Han, Q., Kissinger, C. R., Showalter, R. E., Lardy, M., Shah, A. M., Tsan, M., Patel, R., LeBrun, L. A., Kamran, R., Bartkowski, D. M., Nolan, T. G., Norris, D. A., Sergeeva, M. V. & Kirkovsky, L. (2008). *Bioorg Med Chem Lett* **18**, 4628-4632.

Ferrer-Orta, C., Arias, A., Agudo, R., Perez-Luque, R., Escarmis, C., Domingo, E. & Verdaguer, N. (2006). *EMBO J* **25**, 880-888.

Ferrer-Orta, C., Arias, A., Perez-Luque, R., Escarmis, C., Domingo, E. & Verdaguer, N. (2007). *Proc Natl Acad Sci U S A* **104**, 9463-9468.

Ferrer-Orta, C., de la Higuera, I., Caridi, F., Sanchez-Aparicio, M. T., Moreno, E., Perales, C., Singh, K., Sarafianos, S. G., Sobrino, F., Domingo, E. & Verdaguer, N. (2015). *J Virol* **89**, 6848-6859.

Ferrero, D. S., Buxaderas, M., Rodriguez, J. F. & Verdaguer, N. (2015). *PLoS Pathog* **11**, e1005265.

Garriga, D., Navarro, A., Querol-Audi, J., Abaitua, F., Rodriguez, J. F. & Verdaguer, N. (2007). *Proc Natl Acad Sci U S A* **104**, 20540-20545.

Graham, S. C., Sarin, L. P., Bahar, M. W., Myers, R. A., Stuart, D. I., Bamford, D. H. & Grimes, J. M. (2011). *PLoS Pathog* **7**, e1002085.

Gruez, A., Selisko, B., Roberts, M., Bricogne, G., Bussetta, C., Jabafi, I., Coutard, B., De Palma, A. M., Neyts, J. & Canard, B. (2008). *J Virol* **82**, 9577-9590.

Hang, J. Q., Yang, Y., Harris, S. F., Leveque, V., Whittington, H. J., Rajyaguru, S., Ao-Ieong, G., McCown, M. F., Wong, A., Giannetti, A. M., Le Pogam, S., Talamas, F., Cammack, N., Najera, I. & Klumpp, K. (2009). *J Biol Chem* **284**, 15517-15529.

Harrus, D., Ahmed-El-Sayed, N., Simister, P. C., Miller, S., Triconnet, M., Hagedorn, C. H., Mahias, K., Rey, F. A., Astier-Gin, T. & Bressanelli, S. (2010). *J Biol Chem* **285**, 32906-32918.

Hengrung, N., El Omari, K., Serna Martin, I., Vreede, F. T., Cusack, S., Rambo, R. P., Vonrhein, C., Bricogne, G., Stuart, D. I., Grimes, J. M. & Fodor, E. (2015). *Nature* **527**, 114-117.

Ikegashira, K., Oka, T., Hirashima, S., Noji, S., Yamanaka, H., Hara, Y., Adachi, T., Tsuruha, J., Doi, S., Hase, Y., Noguchi, T., Ando, I., Ogura, N., Ikeda, S. & Hashimoto, H. (2006). *J Med Chem* **49**, 6950-6953.

Kim, S. H., Tran, M. T., Ruebsam, F., Xiang, A. X., Ayida, B., McGuire, H., Ellis, D., Blazel, J., Tran, C. V., Murphy, D. E., Webber, S. E., Zhou, Y., Shah, A. M., Tsan, M., Showalter, R. E., Patel, R., Gobbi, A., LeBrun, L. A., Bartkowski, D. M., Nolan, T. G., Norris, D. A., Sergeeva, M. V., Kirkovsky, L., Zhao, Q., Han, Q. & Kissinger, C. R. (2008). *Bioorg Med Chem Lett* **18**, 4181-4185.

Kumar, D. V., Rai, R., Brameld, K. A., Somoza, J. R., Rajagopalan, R., Janc, J. W., Xia, Y. M., Ton, T. L., Shaghafi, M. B., Hu, H., Lehoux, I., To, N., Young, W. B. & Green, M. J. (2011). *Bioorg Med Chem Lett* **21**, 82-87.

Lam, A. M., Edwards, T. E., Mosley, R. T., Murakami, E., Bansal, S., Lugo, C., Bao, H., Otto, M. J., Sofia, M. J. & Furman, P. A. (2014). *Antimicrob Agents Chemother* **58**, 6861-6869.

LaPlante, S. R., Gillard, J. R., Jakalian, A., Aubry, N., Coulombe, R., Brochu, C., Tsantrizos, Y. S., Poirier, M., Kukolj, G. & Beaulieu, P. L. (2010). *J Am Chem Soc* **132**, 15204-15212.

Le Pogam, S., Kang, H., Harris, S. F., Leveque, V., Giannetti, A. M., Ali, S., Jiang, W. R., Rajyaguru, S., Tavares, G., Oshiro, C., Hendricks, T., Klumpp, K., Symons, J., Browner, M. F., Cammack, N. & Najera, I. (2006). *J Virol* **80**, 6146-6154.

Lee, J. H., Alam, I., Han, K. R., Cho, S., Shin, S., Kang, S., Yang, J. M. & Kim, K. H. (2011). *J Gen Virol* **92**, 1607-1616.

Lesburg, C. A., Cable, M. B., Ferrari, E., Hong, Z., Mannarino, A. F. & Weber, P. C. (1999). *Nat Struct Biol* **6**, 937-943.

Li, H., Tatlock, J., Linton, A., Gonzalez, J., Borchardt, A., Dragovich, P., Jewell, T., Prins, T., Zhou, R., Blazel, J., Parge, H., Love, R., Hickey, M., Doan, C., Shi, S., Duggal, R., Lewis, C. & Fuhrman, S. (2006). *Bioorg Med Chem Lett* **16**, 4834-4838.

Li, H., Tatlock, J., Linton, A., Gonzalez, J., Jewell, T., Patel, L., Ludlum, S., Drowns, M., Rahavendran, S. V., Skor, H., Hunter, R., Shi, S. T., Herlihy, K. J., Parge, H., Hickey, M., Yu, X., Chau, F., Nonomiya, J. & Lewis, C. (2009). *J Med Chem* **52**, 1255-1258.

Li, L. S., Zhou, Y., Murphy, D. E., Stankovic, N., Zhao, J., Dragovich, P. S., Bertolini, T., Sun, Z., Ayida, B., Tran, C. V., Ruebsam, F., Webber, S. E., Shah, A. M., Tsan, M., Showalter, R. E., Patel, R., Lebrun, L. A., Bartkowski, D. M., Nolan, T. G., Norris, D. A., Kamran, R., Brooks, J., Sergeeva, M. V., Kirkovsky, L., Zhao, Q. & Kissinger, C. R. (2008). *Bioorg Med Chem Lett* **18**, 3446-3455.

Lim, S. P., Koh, J. H., Seh, C. C., Liew, C. W., Davidson, A. D., Chua, L. S., Chandrasekaran, R., Cornvik, T. C., Shi, P. Y. & Lescar, J. (2013). *J Biol Chem* **288**, 31105-31114.

Love, R. A., Parge, H. E., Yu, X., Hickey, M. J., Diehl, W., Gao, J., Wriggers, H., Ekker, A., Wang, L., Thomson, J. A., Dragovich, P. S. & Fuhrman, S. A. (2003). *J Virol* **77**, 7575-7581.

Marcotte, L. L., Wass, A. B., Gohara, D. W., Pathak, H. B., Arnold, J. J., Filman, D. J., Cameron, C. E. & Hogle, J. M. (2007). *J Virol* **81**, 3583-3596.

Martin Hernando, J. I., Ontoria, J. M., Malancona, S., Attenni, B., Fiore, F., Bonelli, F., Koch, U., Di Marco, S., Colarusso, S., Ponzi, S., Gennari, N., Vignetti, S. E., Del Rosario Rico Ferreira, M., Habermann, J., Rowley, M. & Narjes, F. (2009). *ChemMedChem* **4**, 1695-1713.

Maynard, A., Crosby, R. M., Ellis, B., Hamatake, R., Hong, Z., Johns, B. A., Kahler, K. M., Koble, C., Leivers, A., Leivers, M. R., Mathis, A., Peat, A. J., Pouliot, J. J., Roberts, C. D., Samano, V., Schmidt, R. M., Smith, G. K., Spaltenstein, A., Stewart, E. L., Thommes, P., Turner, E. M., Voitenleitner, C., Walker, J. T., Waitt, G., Weatherhead, J., Weaver, K., Williams, S., Wright, L., Xiong, Z. Z., Haigh, D. & Shotwell, J. B. (2014). *J Med Chem* **57**, 1902-1913.

Mosley, R. T., Edwards, T. E., Murakami, E., Lam, A. M., Grice, R. L., Du, J., Sofia, M. J., Furman, P. A. & Otto, M. J. (2012). *J Virol* **86**, 6503-6511.

Moustafa, I. M., Korboukh, V. K., Arnold, J. J., Smidansky, E. D., Marcotte, L. L., Gohara, D. W., Yang, X., Sanchez-Farran, M. A., Filman, D., Maranas, J. K., Boehr, D. D., Hogle, J. M., Colina, C. M. & Cameron, C. E. (2014). *J Biol Chem* **289**, 36229-36248.

Narjes, F., Crescenzi, B., Ferrara, M., Habermann, J., Colarusso, S., Ferreira Mdel, R., Stansfield, I., Mackay, A. C., Conte, I., Ercolani, C., Zaramella, S., Palumbi, M. C., Meuleman, P., Leroux-Roels, G., Giuliano, C., Fiore, F., Di Marco, S., Baiocco, P., Koch, U., Migliaccio, G., Altamura, S., Laufer, R., De Francesco, R. & Rowley, M. (2011). *J Med Chem* **54**, 289-301.

Ng, K. K., Cherney, M. M., Vazquez, A. L., Machin, A., Alonso, J. M., Parra, F. & James, M. N. (2002). *J Biol Chem* **277**, 1381-1387.

Ng, K. K., Pendas-Franco, N., Rojo, J., Boga, J. A., Machin, A., Alonso, J. M. & Parra, F. (2004). *J Biol Chem* **279**, 16638-16645.

Noble, C. G., Lim, S. P., Arora, R., Yokokawa, F., Nilar, S., Seh, C. C., Wright, S. K., Benson, T. E., Smith, P. W. & Shi, P. Y. (2016). *J Biol Chem* **291**, 8541-8548.

Noble, C. G., Lim, S. P., Chen, Y. L., Liew, C. W., Yap, L., Lescar, J. & Shi, P. Y. (2013). *J Virol* **87**, 5291-5295.

O'Farrell, D., Trowbridge, R., Rowlands, D. & Jager, J. (2003). *J Mol Biol* **326**, 1025-1035.

Ontoria, J. M., Rydberg, E. H., Di Marco, S., Tomei, L., Attenni, B., Malancona, S., Martin Hernando, J. I., Gennari, N., Koch, U., Narjes, F., Rowley, M., Summa, V., Carroll, S. S., Olsen, D. B., De Francesco, R., Altamura, S., Migliaccio, G. & Carfi, A. (2009). *J Med Chem* **52**, 5217-5227.

Pan, J., Vakharia, V. N. & Tao, Y. J. (2007). *Proc Natl Acad Sci U S A* **104**, 7385-7390.

Poranen, M. M., Salgado, P. S., Koivunen, M. R., Wright, S., Bamford, D. H., Stuart, D. I. & Grimes, J. M. (2008). *Nucleic Acids Res* **36**, 6633-6644.

Powers, J. P., Piper, D. E., Li, Y., Mayorga, V., Anzola, J., Chen, J. M., Jaen, J. C., Lee, G., Liu, J., Peterson, M. G., Tonn, G. R., Ye, Q., Walker, N. P. & Wang, Z. (2006). *J Med Chem* **49**, 1034-1046.

Qian, X., Hamid, F. M., El Sahili, A., Darwis, D. A., Wong, Y. H., Bhushan, S., Makeyev, E. V. & Lescar, J. (2016). *J Biol Chem* **291**, 9295-9309.

Ruebsam, F., Murphy, D. E., Tran, C. V., Li, L. S., Zhao, J., Dragovich, P. S., McGuire, H. M., Xiang, A. X., Sun, Z., Ayida, B. K., Blazel, J. K., Kim, S. H., Zhou, Y., Han, Q., Kissinger, C. R., Webber, S. E., Showalter, R. E., Shah, A. M., Tsan, M., Patel, R. A., Thompson, P. A., Lebrun, L. A., Hou, H. J., Kamran, R., Sergeeva, M. V., Bartkowski, D. M., Nolan, T. G., Norris, D. A., Khandurina, J., Brooks, J., Okamoto, E. & Kirkovsky, L. (2009). *Bioorg Med Chem Lett* **19**, 6404-6412.

Ruebsam, F., Webber, S. E., Tran, M. T., Tran, C. V., Murphy, D. E., Zhao, J., Dragovich, P. S., Kim, S. H., Li, L. S., Zhou, Y., Han, Q., Kissinger, C. R., Showalter, R. E., Lardy, M., Shah, A. M., Tsan, M., Patel, R., Lebrun, L. A., Kamran, R., Sergeeva, M. V., Bartkowski, D. M., Nolan, T. G., Norris, D. A. & Kirkovsky, L. (2008). *Bioorg Med Chem Lett* **18**, 3616-3621.

Schoenfeld, R. C., Bourdet, D. L., Brameld, K. A., Chin, E., de Vicente, J., Fung, A., Harris, S. F., Lee, E. K., Le Pogam, S., Leveque, V., Li, J., Lui, A. S., Najera, I., Rajyaguru, S., Sangi, M., Steiner, S., Talamas, F. X., Taygerly, J. P. & Zhao, J. (2013). *J Med Chem* **56**, 8163-8182.

Scrima, N., Caillet-Saguy, C., Ventura, M., Harrus, D., Astier-Gin, T. & Bressanelli, S. (2012). *J Virol* **86**, 7107-7117.

Sholders, A. J. & Peersen, O. B. (2014). *J Mol Biol* **426**, 1407-1419.

Simister, P., Schmitt, M., Geitmann, M., Wicht, O., Danielson, U. H., Klein, R., Bressanelli, S. & Lohmann, V. (2009). *J Virol* **83**, 11926-11939.

Slater, M. J., Amphlett, E. M., Andrews, D. M., Bravi, G., Burton, G., Cheasty, A. G., Corfield, J. A., Ellis, M. R., Fenwick, R. H., Fernandes, S., Guidetti, R., Haigh, D., Hartley, C. D., Howes, P. D., Jackson, D. L., Jarvest, R. L., Lovegrove, V. L., Medhurst, K. J., Parry, N. R., Price, H., Shah, P., Singh, O. M., Stocker, R., Thommes, P., Wilkinson, C. & Wonacott, A. (2007). *J Med Chem* **50**, 897-900.

Surana, P., Satchidanandam, V. & Nair, D. T. (2014). *Nucleic Acids Res* **42**, 2758-2773.

Talamas, F. X., Abbot, S. C., Anand, S., Brameld, K. A., Carter, D. S., Chen, J., Davis, D., de Vicente, J., Fung, A. D., Gong, L., Harris, S. F., Inbar, P., Labadie, S. S., Lee, E. K., Lemoine, R., Le Pogam, S., Leveque, V., Li, J., McIntosh, J., Najera, I., Park, J., Railkar, A., Rajyaguru, S., Sangi, M., Schoenfeld, R. C., Staben, L. R., Tan, Y., Taygerly, J. P., Villasenor, A. G. & Weller, P. E. (2014). *J Med Chem* **57**, 1914-1931.

Talamas, F. X., Ao-Ieong, G., Brameld, K. A., Chin, E., de Vicente, J., Dunn, J. P., Ghate, M., Giannetti, A. M., Harris, S. F., Labadie, S. S., Leveque, V., Li, J., Lui, A. S., McCaleb, K. L., Najera, I., Schoenfeld, R. C., Wang, B. & Wong, A. (2013). *J Med Chem* **56**, 3115-3119.

Tarantino, D., Pezzullo, M., Mastrangelo, E., Croci, R., Rohayem, J., Robel, I., Bolognesi, M. & Milani, M. (2014). *Antiviral Res* **102**, 23-28.

Thompson, A. A., Albertini, R. A. & Peersen, O. B. (2007). *J Mol Biol* **366**, 1459-1474.

Thompson, A. A. & Peersen, O. B. (2004). *EMBO J* **23**, 3462-3471.

van der Linden, L., Vives-Adrian, L., Selisko, B., Ferrer-Orta, C., Liu, X., Lanke, K., Ulferts, R., De Palma, A. M., Tanchis, F., Goris, N., Lefebvre, D., De Clercq, K., Leyssen, P., Lacroix, C., Purstinger, G., Coutard, B., Canard, B., Boehr, D. D., Arnold, J. J., Cameron, C. E., Verdaguer, N., Neyts, J. & van Kuppeveld, F. J. (2015). *PLoS Pathog* **11**, e1004733.

Wang, G., Lei, H., Wang, X., Das, D., Hong, J., Mackinnon, C. H., Coulter, T. S., Montalbetti, C. A., Mears, R., Gai, X., Bailey, S. E., Ruhrmund, D., Hooi, L., Misialek, S., Rajagopalan, P. T., Cheng, R. K., Barker, J. J., Felicetti, B., Schonfeld, D. L., Stoycheva, A., Buckman, B. O., Kossen, K., Seiwert, S. D. & Beigelman, L. (2009). *Bioorg Med Chem Lett* **19**, 4480-4483.

Wang, M., Ng, K. K., Cherney, M. M., Chan, L., Yannopoulos, C. G., Bedard, J., Morin, N., Nguyen-Ba, N., Alaoui-Ismaili, M. H., Bethell, R. C. & James, M. N. (2003). *J Biol Chem* **278**, 9489-9495.

Wright, S., Poranen, M. M., Bamford, D. H., Stuart, D. I. & Grimes, J. M. (2012). *J Virol* **86**, 2837-2849.

Wu, Y., Lou, Z., Miao, Y., Yu, Y., Dong, H., Peng, W., Bartlam, M., Li, X. & Rao, Z. (2010). *Protein Cell* **1**, 491-500.

Yan, S., Appleby, T., Gunic, E., Shim, J. H., Tasu, T., Kim, H., Rong, F., Chen, H., Hamatake, R., Wu, J. Z., Hong, Z. & Yao, N. (2007). *Bioorg Med Chem Lett* **17**, 28-33.

Yan, S., Appleby, T., Larson, G., Wu, J. Z., Hamatake, R., Hong, Z. & Yao, N. (2006). *Bioorg Med Chem Lett* **16**, 5888-5891.

Yan, S., Appleby, T., Larson, G., Wu, J. Z., Hamatake, R. K., Hong, Z. & Yao, N. (2007). *Bioorg Med Chem Lett* **17**, 1991-1995.

Yan, S., Larson, G., Wu, J. Z., Appleby, T., Ding, Y., Hamatake, R., Hong, Z. & Yao, N. (2007). *Bioorg Med Chem Lett* **17**, 63-67.

Yang, H., Hendricks, R. T., Arora, N., Nitzan, D., Yee, C., Lucas, M. C., Yang, Y., Fung, A., Rajyaguru, S., Harris, S. F., Leveque, V. J., Hang, J. Q., Pogam, S. L., Reuter, D. & Tavares, G. A. (2010). *Bioorg Med Chem Lett* **20**, 4614-4619.

Yap, T. L., Xu, T., Chen, Y. L., Malet, H., Egloff, M. P., Canard, B., Vasudevan, S. G. & Lescar, J. (2007). *J Virol* **81**, 4753-4765.

Zhao, Y., Soh, T. S., Zheng, J., Chan, K. W., Phoo, W. W., Lee, C. C., Tay, M. Y., Swaminathan, K., Cornvik, T. C., Lim, S. P., Shi, P. Y., Lescar, J., Vasudevan, S. G. & Luo, D. (2015). *PLoS Pathog* **11**, e1004682.

Zhou, Y., Webber, S. E., Murphy, D. E., Li, L. S., Dragovich, P. S., Tran, C. V., Sun, Z., Ruebsam, F., Shah, A. M., Tsan, M., Showalter, R. E., Patel, R., Li, B., Zhao, Q., Han, Q., Hermann, T., Kissinger, C. R., Lebrun, L., Sergeeva, M. V. & Kirkovsky, L. (2008). *Bioorg Med Chem Lett* **18**, 1413-1418.